RESEARCH

Multi-omics analysis reveals a feedback loop amplifying immune responses in acute graft-versus-host disease due to imbalanced gut microbiota and bile acid metabolism

Lijie Han[1,2†], Xianlei Sun[3†], Jingjing Kong[1,2†], Jin Li[1,2], Kai Feng[2], Yanliang Bai[4], Xianjing Wang[5], Zhenhua Zhu[6], Fengyuan Yang[3], Qingzhou Chen[6], Mengmeng Zhang[1,2], Baohong Yue[6], Xiaoqian Wang[6], Liyan Fu[7], Yaoyao Chen[6], Qiankun Yang[8], Shuya Wang[8], Qingxuan Xin[7], Nannan Sun[1,2], Danfeng Zhang[1,2], Yiwei Zhou[1,2], Yanxia Gao[9], Junwei Zhao[6*], Yong Jiang[10*] and Rongqun Guo[1,2*]

Abstract

Acute graft-versus-host disease (aGVHD) is primarily driven by allogeneic donor T cells associated with an altered composition of the host gut microbiome and its metabolites. The severity of aGVHD after allogeneic hematopoietic stem cell transplantation (allo-HSCT) is not solely determined by the host and donor characteristics; however, the underlying mechanisms remain unclear. Using single-cell RNA sequencing, we decoded the immune cell atlas of 12 patients who underwent allo-HSCT: six with aGVHD and six with non-aGVHD. We performed a fecal microbiota (16SrRNA sequencing) analysis to investigate the fecal bacterial composition of 82 patients: 30 with aGVHD and 52 with non-aGVHD. Fecal samples from these patients were analyzed for bile acid metabolism. Through multi-omic analysis, we identified a feedback loop involving "immune cell-gut microbes-bile acid metabolites" contributing to heightened immune responses in patients with aGVHD. The dysbiosis of the gut microbiota and disruption of bile acid metabolism contributed to an exaggerated interleukin-1 mediated immune response. Our findings suggest that resistin and defensins are crucial in mitigating against aGVHD. Therefore, a comprehensive multi-omic atlas incorporating immune cells, gut microbes, and bile acid metabolites was developed in this study and used to propose novel, non-immunosuppressive approaches to prevent aGVHD.

†Lijie Han, Xianlei Sun and Jingjing Kong contributed equally to this work.

*Correspondence:
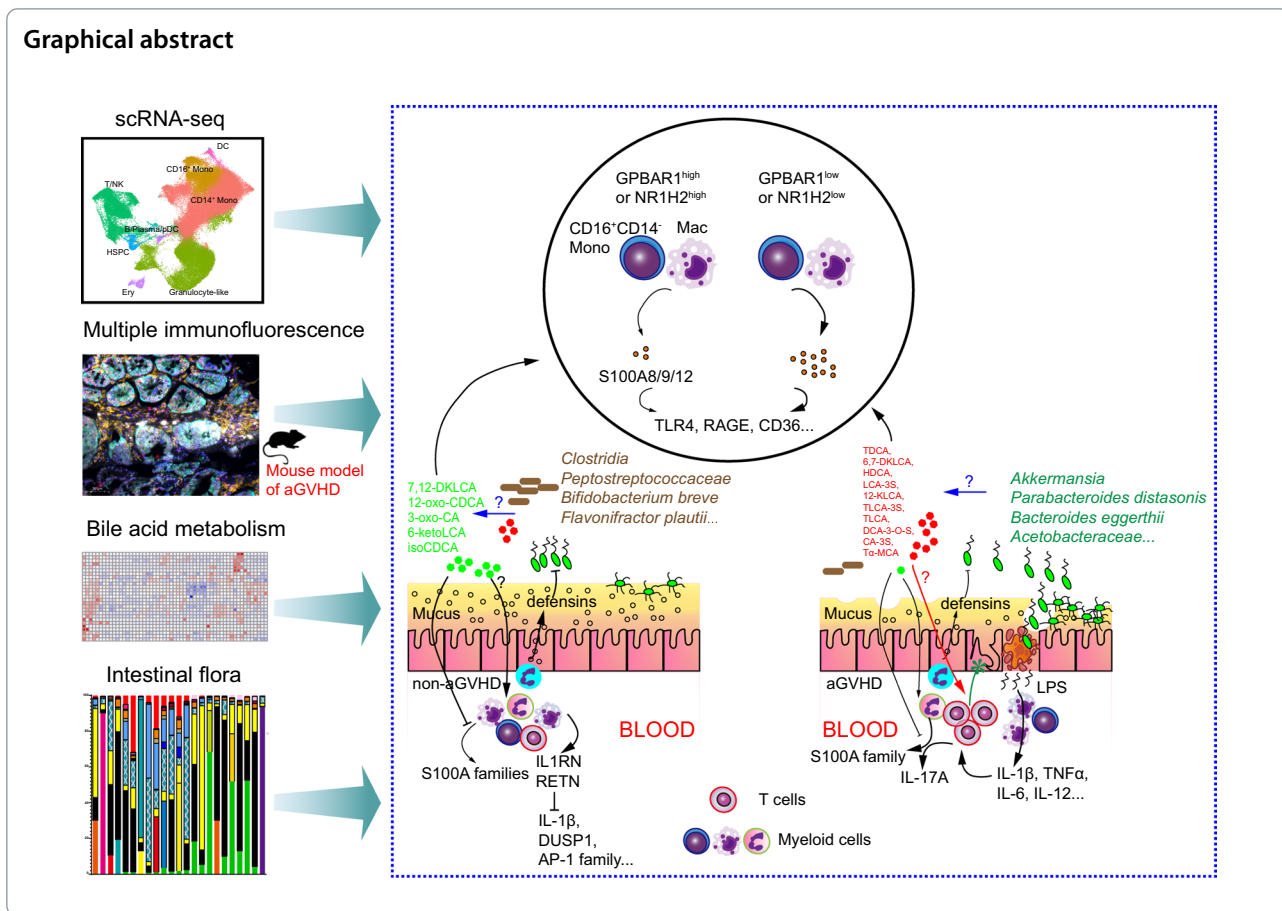Junwei Zhao
junweizhao@alumni.sjtu.edu.cn
Yong Jiang
jiang48231@163.com
Rongqun Guo
guorq2007@163.com
Full list of author information is available at the end of the article

Han *et al. Journal of Translational Medicine*   (2024) 22:746

Page 2 of 24

Graphical abstract

Introduction

Many compounds possess powerful anticancer activities with side effects [1–3]. Allogeneic hematopoietic stem cell transplantation (allo-HSCT) is a viable treatment option for malignant hematological diseases and bone marrow failure; however, patients undergoing allo-HSCT are at significant risk of acute graft-versus-host disease (aGVHD), which can lead to severe complications and even death. The liver and gastrointestinal tract are commonly attacked by allogeneic donor T-cells. Current treatment approaches often fail to effectively mitigate against aGVHD progression.

The activation of donor-derived allogeneic T cells by the host antigen-presenting cells (APCs) is a crucial step in aGVHD development. Activated T-cells target and kill epithelial cells, whereas myeloid cells are recruited to the ileum to address tissue damage and microbial infection. Myeloid cell-derived IL-12 enhances the secretion of IFN-γ by lamina propria lymphocytes, leading to increased expression of MHC class II on intestinal epithelial cells, thereby promoting the development of CD4^{+} T cell-dependent GVHD [4]. The administration of antibiotics is important for patients undergoing allo-HSCT [5,

6]. Allogeneic immune responses, high dose chemotherapy, and total body irradiation contribute to the translocation of lipopolysaccharide (LPS) into the systemic circulation, resulting in the production of inflammatory cytokines, such as TNF-α and IL-1β by macrophages [7]. Inflammatory cytokines, including IL-1, IL-6, and TNF-α, augment the host APCs in presenting alloantigens to donor T cells [8]. The precise roles of IFN-α/β in GVHD are not definitively understood when compared with the more destructive role of IFN-γ [9]. Intestinal microbiota and their metabolites are increasingly recognized as significant contributors to GVHD development [10]. Notably, bacterial MHC-II inducers can be suppressed by vancomycin, thereby inhibiting CD4^{+} T cell-mediated GVHD development [11]. Various microbial metabolites, such as bile acids, indole derivatives, and short-chain fatty acids contribute to the immune modulation of GVHD [12]. However, there is a paucity of systematic and comprehensive research on the relationships between the immune cell atlas, microbiome atlas, and bile acid metabolism profiles of patients with aGVHD.

In the present study, we demonstrated that allo-HSCT patients with non-aGVHD exhibit distinct immune

responses characterized by type I IFN-regulation, including the upregulation of *IRF1/7*, as determined through single-cell RNA sequencing (scRNA-seq) analysis. Furthermore, we identified LILRB1, LILRB2, and LILRB4 as crucial markers for the regulation of aGVHD, with hyperactivated AP-1 activation serving as the driving force behind of hyperactivated allogeneic immune responses. IL1-associated molecular patterns are modulated in immune cells from patients with aGVHD through the upregulation of IL1B, IL1R2, IL1R1, and IL1RAP, and the downregulation of IL1RN. Additionally, RETN, which encodes resistin with antibacterial properties, was found to be upregulated in granulocyte-like cells from patients with non-aGVHD. Furthermore, central regulators of allogeneic T cell activation, including *FOS*, *JUN*, *TSC22D3*, *DUSP1*, *DUSP2*, *ZFP36L2*, *GZMK*, *CD52*, *CD27*, *CD28*, *TNFAIP3*, and *IKZF3*, were identified. Notably, T cells from patients with non-aGVHD exhibited high expression levels of *KIR3DL2*, *S1PR5*, *GNLY*, *ADGRG1*, *LGALS1*, *IFITM2*, and *ISG15*. Multiple alterations in immune regulation were observed in the innate immune response associated infections contributing to the pathogenesis of aGVHD. Analysis of 16s rRNA gene sequencing revealed an enrichment of Clostridia and *Peptostreptococcaceae* in fecal samples from patients with non-aGVHD, while *Akkermansiaceae* was enriched in individuals with aGVHD. These changes in microbial composition disrupted bile acid metabolism, potentially reducing the antibacterial capacity of defensins and exacerbating inflammation through pathogens and members of S100A family. These results highlight the significance of the feedback loop involving immune cell-microbiota and its metabolites interactions in the development of aGVHD.

Results

Cellular atlas of immune cells of patients who underwent allo-HSCT presented with and without aGVHD symptoms

Using scRNA-seq to analyze the inherent programming of immune cell types, we analyzed the molecular characteristics of immune cells from six patients who underwent allo-HSCT and developed aGVHD, as well as from six patients who did not develop aGVHD. To validate the cell types, inferences were made by evaluating the relative expression of lineage-specific genes (Supplementary Figure 1A). Through unsupervised clustering analysis of the scRNA-seq dataset from the 12 patients, eight clusters were identified (Fig. 1A). No significant differences were observed in the proportions of most cell types, exception of dendritic cell (DC), hematopoietic stem and progenitor cells (HSPCs), and erythroid subsets (Fig. 1B).

To validate both the established and potential functions of immune regulation in patients with non-aGVHD, we conducted differential gene expression analysis in peripheral blood mononuclear cells (PBMCs) from two groups (non-aGVHD vs. aGVHD). Subsequently, gene ontology (GO) analysis was performed using the upregulated genes in patients with non-aGVHD, revealing the enrichment of differentially expressed genes (DEGs) in biological pathways related to immune response and microbe-related immune regulation (Fig. 1C). Subsequently, we analyzed the expression levels of genes associated with the "immune response-regulating signaling pathway" (Supplementary Figure 1B), and identified key genes involved in immune regulation, including IRF7, IRF1, NLRC4, LILRB4, LILRB1, and LILRB2 (Fig. 1D). Notably, VDR enhances NLRC4 activation to combat intracellular bacterial infections [13]. Additionally, IRF7 serves as a pivotal regulator of the production and secretion of interferon (IFN) type I, essential for defense against infections [14, 15]. The significance of Type I IFN signaling in suppressing activated autologous T cells in patients with aGVHD, as well as the inhibitory effect of LILRB4 on T cell production of IFN-γ, has been documented [16]. Furthermore, the high affinity of LILRB1 and LILRB2 for HLA-G underscores their crucial roles in promoting transplantation tolerance [17]. The KEGG analysis revealed that upregulated genes in patients with non-aGVHD were enriched in pathways related to pathogen-removal pathways (Supplemental Figure 1C). These results suggested that an enhanced innate immune response for pathogen clearance is essential for mitigating against aGVHD (Supplementary Figure 1D).

(See figure on next page.)

Fig. 1 scRNA-seq analysis of PBMCs of patients who underwent allo-HSCT revealing immune regulation signature in aGVHD. **A** Unsupervised clustering (UMAP plot) of scRNA-seq data from PBMCs of patients with aGVHD and with non-aGVHD, with cell subtypes labeled. **B** The frequency percentage of the main cell subtypes (patients with non-aGVHD, n = 6; patients with aGVHD, n = 6). **C** Dot graph illustrating the GO analysis of upregulated genes in PBMCs of patients with non-aGVHD compared with those from individuals with aGVHD. **D** Dot plots illustrating relative expression levels of the upregulated genes *IRF7*, *IRF1*, *NLRC4*, *LILRB1*, *LILRB2*, and *LILRB4* in PBMCs of patients with non-aGVHD. **E** Dot graph illustrating the GO analysis of upregulated genes in PBMCs from patients with aGVHD compared with those from individuals with non-aGVHD. **F** Dot plots were used to display the relative expression levels of downregulated genes (*JUNB*, *FOS*, *JUN*, *CD83*, and *EGR1*) in PBMCs of patients with non-aGVHD. **G** Representative immunofluorescence staining of c-FOS, c-JUN, IRF7 and CD45 in small intestine of control or aGVHD mouse model groups. Scale bar, 20 μm
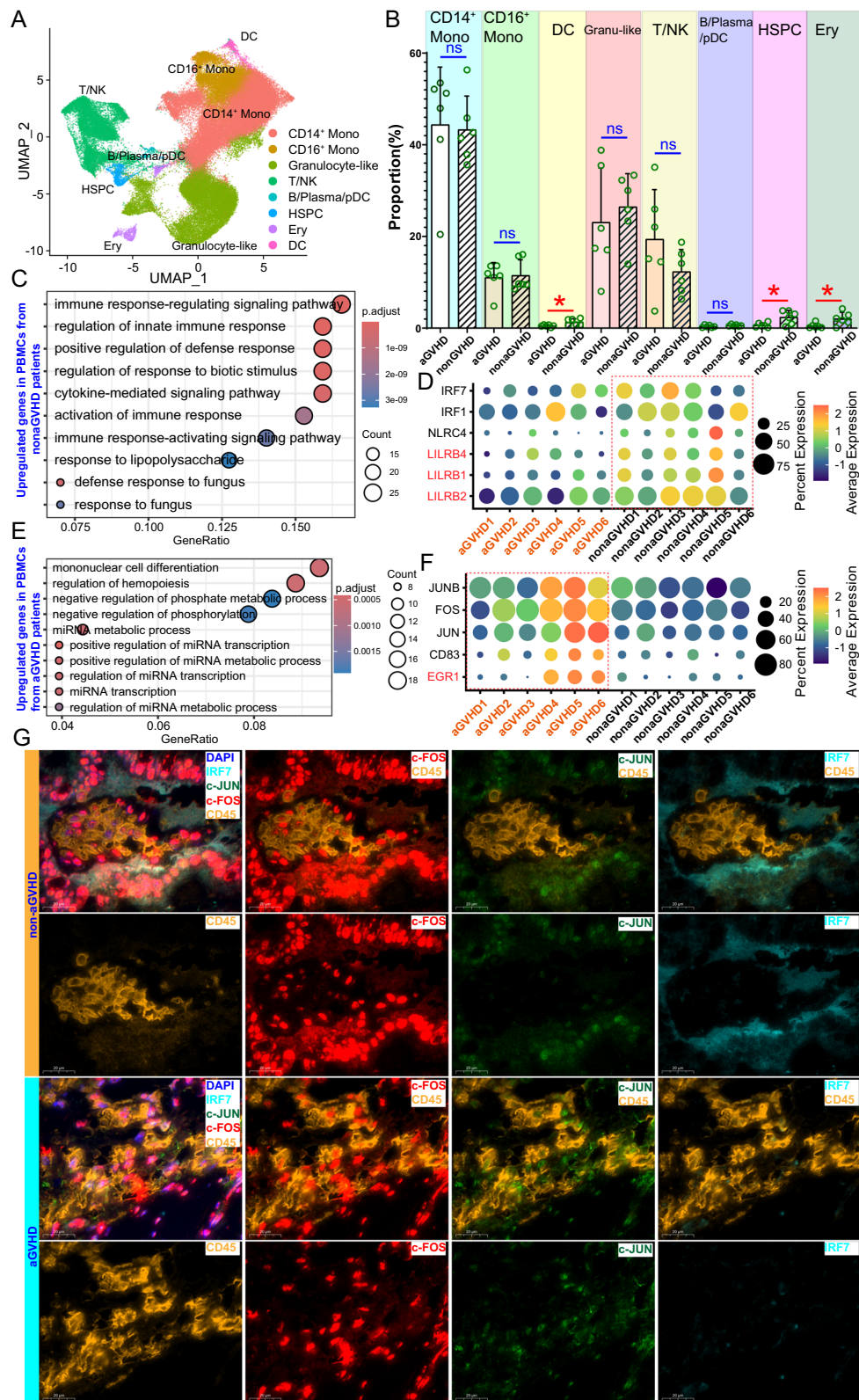
Han *et al. Journal of Translational Medicine*   (2024) 22:746

Page 4 of 24

Fig. 1 (See legend on previous page.)

Han *et al. Journal of Translational Medicine*   (2024) 22:746

Page 5 of 24

Genes that were upregulated in the PBMCs of patients with aGVHD were significantly enriched in pathways related to mononuclear cell differentiation, phosphorylation, and microRNAs (Fig. 1E). Subsequently, we generated a graphical representation of the expression levels of genes associated with "mononuclear cell differentiation" (Supplementary Figure 1E) and identified the key genes involved in immune regulation, including *JUNB, FOS, JUN, CD83*, and *EGR1* (Fig. 1F). Notably, JUNB, FOS, and JUN, which are components of the AP-1 complex, have been implicated in various inflammatory disorders and are known to play a role in IL-1β-mediated immune regulation [18]. Additionally, we observed the protein expression levels of IRF7, c-FOS, and c-JUN in the small intestine of the aGVHD mouse model, and identified that CD45$^+$ immune cells of the aGVHD mouse model exhibited higher c-JUN expression than cells in the non-aGVHD group (Fig. 1G). CD83 is a potential diagnostic marker for GVHD and a target for eliminating autoreactive immune and leukemic cells [19, 20]. Increased expression of EGR1 in patients with aGVHD is consistent with previous findings [21]. Furthermore, KEGG analysis revealed that upregulated genes in patients with aGVHD were associated with T cell-mediated immune response (Supplementary Figure 1F). These findings provide insight into the distinct immune characteristics of patients with aGVHD and non-aGVHD.

IL-1 signaling regulation is out of balance in patients with aGVHD

Next, we established a cellular communication network of different cell types (Supplementary Figure 2A), and found that the IL1 signaling network was involved in the immune response of HSPC and granulocyte-like cells (Fig. 2A). Interestingly, HSPCs of patients with non-aGVHD exhibited elevated *IL1B* mRNA level (Fig. 2B(i)). Conversely, lineage-specific cell types from non-aGVHD patients demonstrated significantly higher IL1B expression than those from patients with non-aGVHD (Fig. 1B(i–iv)). Additionally, cells derived from patients with aGVHD displayed increased expression of IL1R2, IL1R1, and IL1RAP than those from patients with non-aGVHD, suggesting the involvement of IL-1 signaling in the aGVHD-related dysregulated immune response. Notably, the cells of patients with non-aGVHD secreted IL1RN, which acted as an inhibitor of IL-1 signaling by competing with IL-1 (Supplementary Figure 2B). IL-1β is predominantly linked to the activation of innate immunity in response to pathogen-associated molecular pattern molecules (PAMPs) and damage-associated molecular pattern molecules (DAMPs).

Measuring C-reactive protein (CRP) and procalcitonin (PCT) levels can aid in distinguishing infections caused by pathogens. Elevated PCT levels indicated potential bacterial infections in patients with aGVHD compared with those in patients with non-aGVHD (Fig. 2C). Subsequently, we observed elevated concentrations of lipopolysaccharides (LPS) in individuals with aGVHD compared with those with non-aGVHD (Fig. 2D). To further investigate the association between LPS and IL-1 signaling, we analyzed publicly available scRNA-seq datasets of LPS-treated PBMCs. Stimulation with LPS caused a significant increase in the expression of IL1B, IL6, and CXCL8 (Fig. 2E). Notably, LPS stimulation altered the expression profiles of genes related to the human leukocyte antigen (HLA) system (Supplementary Figure 2C). Protein levels of TNF-α, IL6, IL1B, IL12, and CXCL8 (IL8) were quantified using ELISA assay. The results of these elevated cytokines in plasma samples from patients with aGVHD were determined (Fig. 2F and Supplementary Figure 2D). These findings support the development of a model illustrating potential IL-1 regulation triggered by PAMPs in the immune cells of patients with aGVHD (Fig. 2G). The observed increase in IL1B, IL1R1, and IL1RAP expression, along with enhanced IL1RN transcription in various cell types, may contribute to the sustained activation of IL-1 signaling and exacerbate the inflammatory response.

Resistin may play a role in immune regulation by inhibiting LPS-mediated inflammation

The upregulation of *RETN* mRNA expression following LPS stimulation, as illustrated in Fig. 2E, suggests the potential involvement of resistin in cellular communication pathways. Specifically, myeloid cell subsets may influence themselves in an autocrine, paracrine, or endocrine manner via the resistin-cap1 axis (Fig. 3A). The treatment of staphylococcus aureus-primed DCs with resistin attenuates T-cell activity and cytokine production [22]. In addition, resistin-primed DCs can expand Tregs and indirectly enhance their suppressive effects [23]. DCs derived from patients with non-aGVHD exhibited elevated levels of CAP1 compared to those derived from patients with aGVHD (Supplementary Figure 3A). Granulocyte-like cells from patients with non-aGVHD demonstrated increased expression of RETN and CAP1 (Fig. 3B), suggesting that resistin produced by granulocyte-like cells may inhibit hyperactivated immune responses via DC and Tregs-mediated regulation. Furthermore, resistin is a bactericidal protein [24], indicating that these resistin-producing cells possess greater antibacterial activity than cells from patients with aGVHD. Indeed, resistin, an antagonist of LPS binding to TLR4, inhibits the production of pro-inflammatory cytokines (such as IL6) induced by LPS [25]. Multiplex immunofluorescence was performed to examine resistin protein
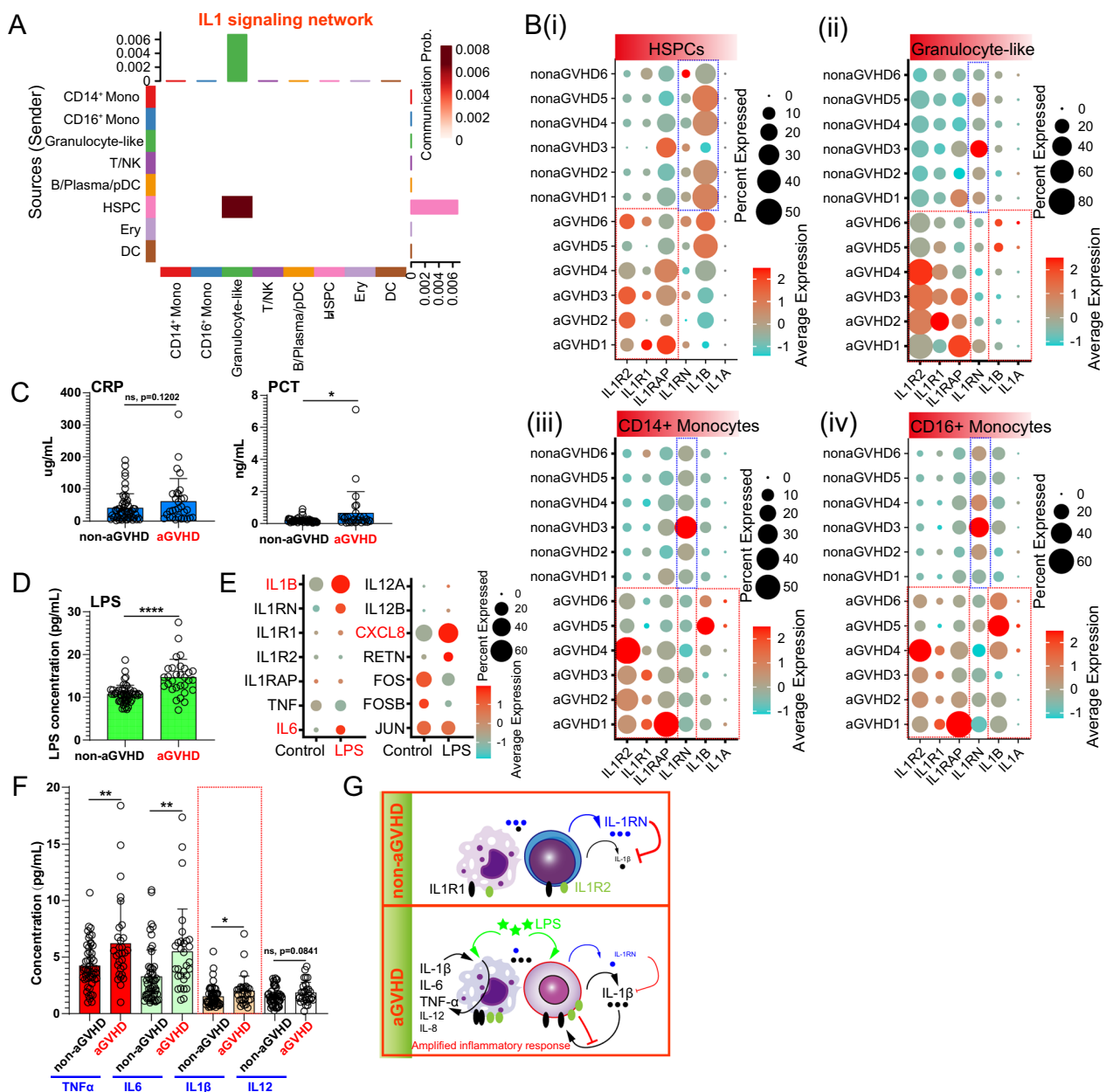
Han *et al. Journal of Translational Medicine*   (2024) 22:746

Page 6 of 24

Fig. 2 Comparison of IL-1 signaling-associated ligands and receptors in individuals with aGVHD and with non-aGVHD. **A** Heatmap of the communication probability of each cluster in the combined dataset of PBMCs of patients undergoing allo-HSCT. **B** The expression levels of *IL1B*, *IL1A*, *IL1R2*, *IL1R1*, *IL1RAP*, and *IL1RN* were assessed in HSPCs (i), granulocyte-like cells (ii), CD14+ monocytes (iii), and CD16+ monocytes (iv) of the participants. **C** The protein expression levels of C-reactive protein (CRP) and procalcitonin (PCT) in patients with aGVHD (n=30) compared to individuals with non-aGVHD (n=52). **D** LPS concentrations were measured using ELISA assay in plasma samples obtained from patients with aGVHD (n=30) and control individuals with non-aGVHD (n=52). **E** Dot plots illustrating the expression levels of specific genes in PBMCs following LPS stimulation. **F** The protein levels of TNF-α, IL6, IL1B, and IL12 were quantified using ELISA assay (patients with non-aGVHD, n=52; patients with aGVHD, n=30). **G** Summary of the IL-1 signaling-associated ligands and receptors identified in the immune cells of patients with aGVHD compared with individuals with non-aGVHD. The activation of IL-1 signaling by LPS and other inflammatory cytokines exacerbates hyperactivated immune responses

expression (Fig. 3C). Consistent with the results of single-cell transcriptome analysis, resistin was significantly downregulated in CD45+ immune cells of the small intestine in the aGVHD mouse model. In experiments utilizing LPS and resistin in THP-1 cell cultures, higher concentrations of resistin effectively suppressed
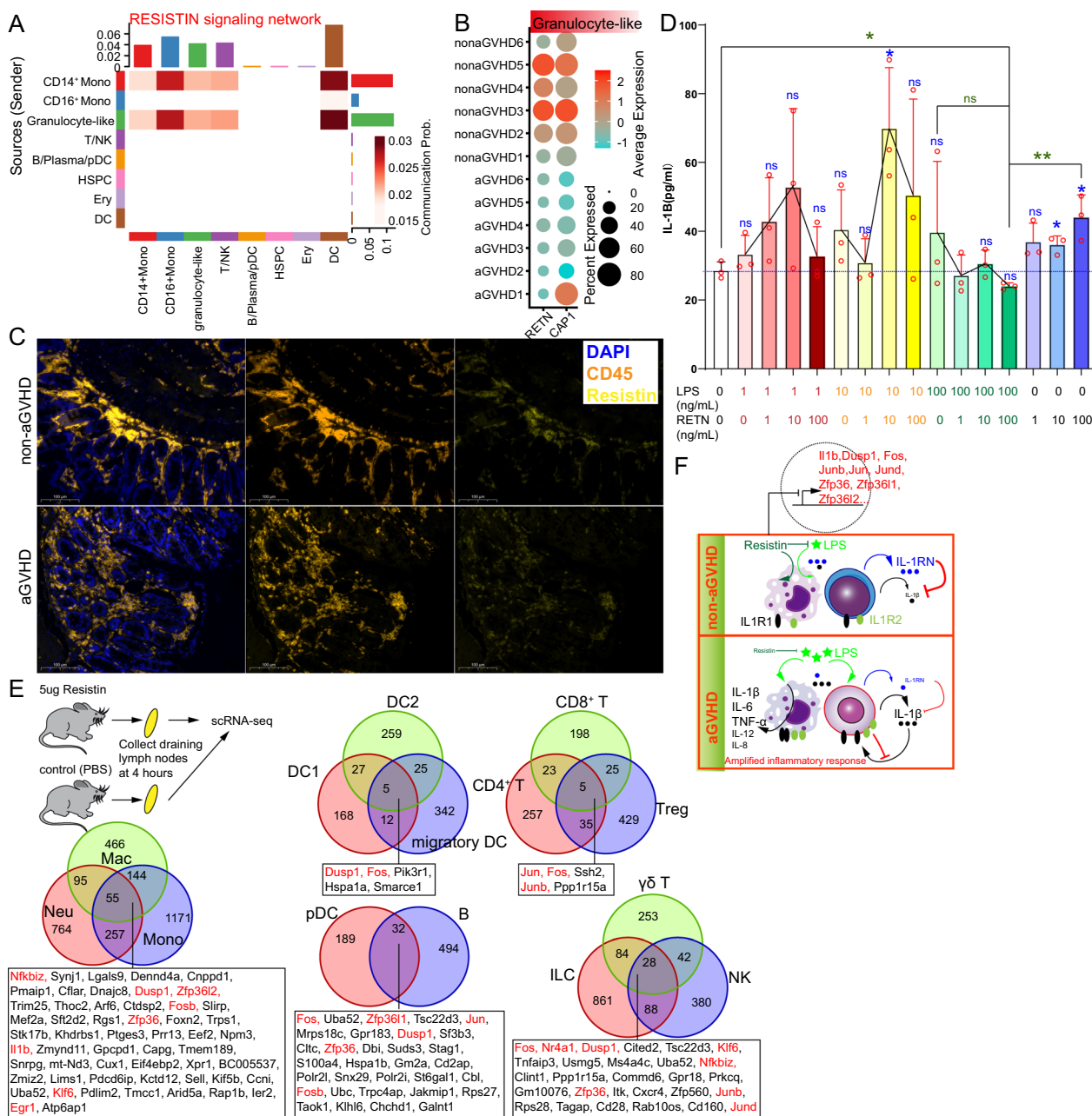
Han *et al. Journal of Translational Medicine*   (2024) 22:746

Page 7 of 24

Fig. 3 Granulocyte-like cells derived from patients with non-aGVHD exhibited elevated levels of RETN expression, suggesting a potential role for resistin in preventing aGVHD. **A** Heatmap display of the communication probability of each cluster within the combined dataset of PBMCs from patients undergoing allo-HSCT. **B** *RETN* and its corresponding receptor *CAP1* were expresed in granulocyte-like cells across each sample. **C** Representative immunofluorescence staining of CD45 and resistin in the small intestine of control or aGVHD mouse model groups. Scale bar, 100 μm. **D** IL-1β concentrations were measured using ELISA assay in cell culture supernatants (n = 3) following various treatments involving LPS and resistin. **E** Venn diagrams illustrating the shared conserved downregulated genes among distinct lineages (group 1: neutrophils vs. macrophages vs. monocytes; group 2: cDC1 vs. cDC2 vs. migratory DC; group 3: plasmacytoid dendritic cell (pDC) vs. B cells; group 4: CD4+ T cells vs. CD8+ T cells vs. Treg; group 5: innate lymphoid cell (ILC) vs. γδ T cells vs. NK cells). **F** Summary of the resistin-driven immune regulation in the presence of LPS or other special conditions

IL-1β production triggered by high concentrations of LPS (Fig. 3D). Additionally, our investigation revealed that resistin plays a role in immune regulation by downregulating the expression of conserved regulatory molecules, including *Dusp1*, members of the AP-1 transcription factor family (*Fos, Junb, Jun,* and *Jund*)

Han *et al. Journal of Translational Medicine*   (2024) 22:746

Page 8 of 24

and members of the ZFP36 family (*Zfp36*, *Zfp36l1*, and *Zfp36l2*) (Fig. 3D and Supplementary Figure 3B), which have potential to mitigate the abnormally high expression of AP-1 families in patients with aGVHD (Fig. 1F). Furthermore, resistin treatment reduced the expression of *Il1b* in myeloid cell lineages, including neutrophils, monocytes, and macrophages, in vivo (Fig. 3E). This indicated that resistin functions beyond its role as an inflammatory cytokine. Additionally, the upregulation of resistin expression may attenuate LPS-induced immune hyperactivation impairment, promoting acceptable immune responses mediated by resistin (Fig. 3F).

Altered gut microbiome structure is involved in the immune responses of patients with aGVHD

Microbe-associated immune regulation-related DEGs (Fig. 1C), elevated LPS levels in patients with aGVHD, abnormal IL1B expression, and increased bactericidal resistin expression prompted an examination of the relationship between microbiome structure and aGVHD. To explore the potential involvement of microbiome structure in immune dysregulation, a comparison was made between the signature gut microorganisms of aGVHD patients and those with non-aGVHD (Supplementary Figure 4A). Characterization of the microbiota composition using 16s ribosomal RNA gene sequencing revealed a significant enrichment of *c. Clostridia* and *f. Peptostreptococcaceae*
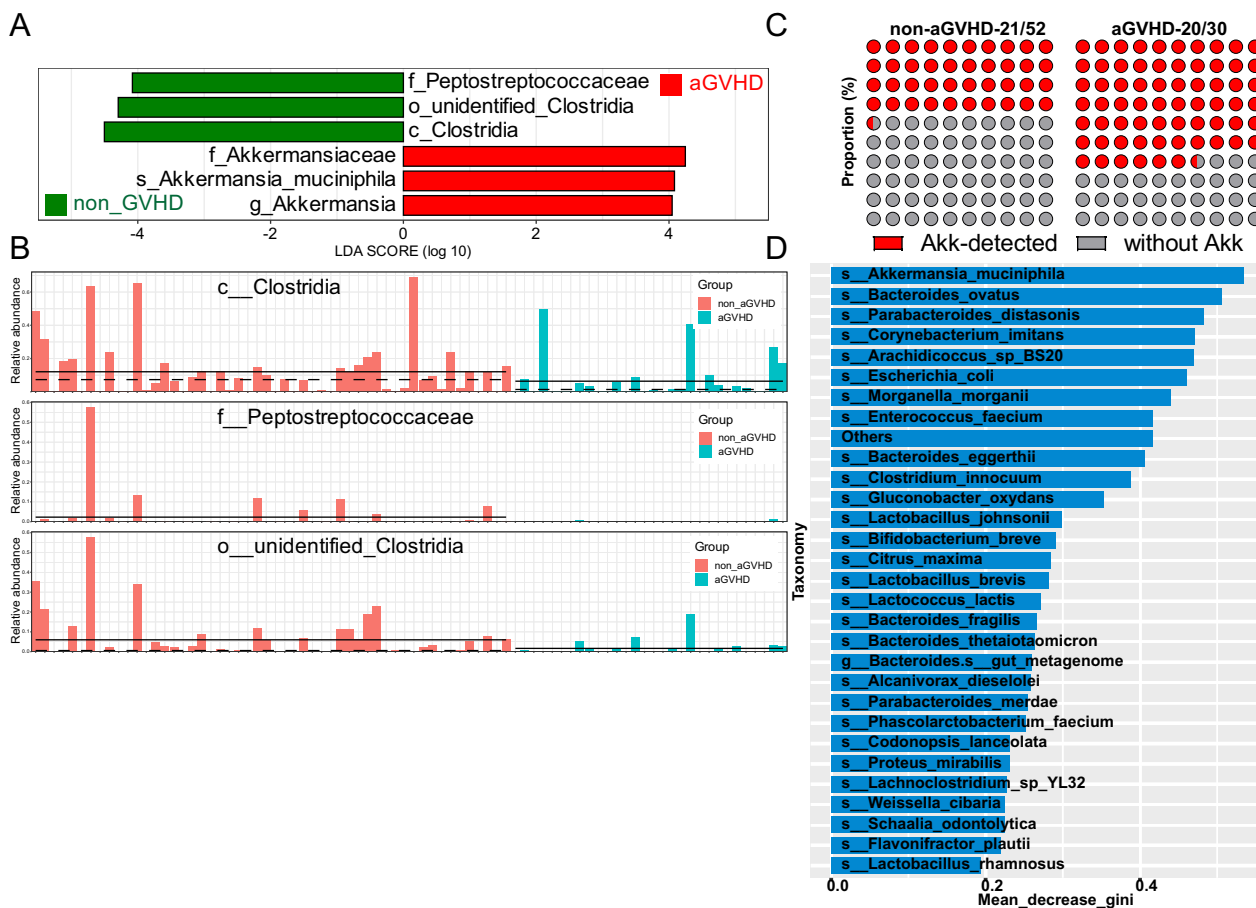

Fig. 4 Patients with aGVHD exhibited dysbiosis in their intestinal microbiota. **A** Linear Discriminant Analysis (LDA) scores of species that exhibit differential abundance between individuals with aGVHD (red) and those with non-aGVHD (green) are examined. The LDA scores serve as a measure of the magnitude of the effect of each abundant species. Species with an LDA score exceeding 4 in either group are deemed enriched in that group. **B** Relative abundance of typical intestinal bacteria enriched in samples obtained from patients with non-aGVHD. **C** The frequencies of samples detecting *Akk.*-related 16s RNA were compared between patients with aGVHD (20 out of 30 samples) and individuals with non-aGVHD (21 out of 52 samples). **D** A random forest model was used to assess the influence of various bacterial species within the intestinal microbiota on the occurrence of aGVHD. The Gini index was used to quantify the significance of each node within the classification tree and compare the variables' importance. The figure displays the top 30 strains ranked based on the average reduction value of the Gini coefficient

in patients with non-aGVHD (Fig. 4A, B). The abundances of *f_Peptostreptococcaceae*, *g_Hungatella* of the *f__Lachnospiraceae*, *Clostridia*, and *s_Flavonifractor_plautii* of the *O_Clostridia* were higher in the non-aGVHD group compared than in aGVHD group (P < 0.05), all of which were classified under the *Firmicutes phylum, Clostridia class*. Additionally, the abundance of *s. Bifidobacterium breve* was significantly higher in the non-aGVHD group than in the aGVHD group (P < 0.05). Other commensal bacteria, such as *f_Akkermansiaceae*, *g_Akkermansia*, *s_Akkermansia muciniphila*, *s_Parabacteroides_distasonis*, *s_Bacteroides_eggerthii*, *f_Acetobacteraceae*, *g_Oscillibacter*, *g_Gryllotalpicola*, *s_Alcanivorax_dieselolei*, *s_Corynebacterium_imitans*, *g_Alcanivorax* and *f_Pseudomonadales*, were significantly higher in abundance in the aGVHD group than in the non-aGVHD group (all P < 0.05). Additionally, *Peptostreptococcus anaerobius* produces the tryptophan metabolite *trans*-3-indoleacrylic acid (IDA), which serves as an endogenous ligand of AHR, and plays a role in immune regulation [26]. AHR plays a crucial role in various immune processes, including bacterial clearance, T cell exhaustion, and the maintenance of a quiescent state necessary for CD8$^+$ T cells memory formation [27, 28]. Furthermore, the AHR pathway is integral to the establishment of a Treg-tolerogenic macrophage suppressive axis and the up-regulation of PD-1 in CD8$^+$ T cells [29]. AHR contributes significantly to endotoxin tolerance and prevents an excessive immune response [30]. Additionally, *Clostridiales* confer protection against pathogen infections in mice [31]. Notably, the frequency of *Akkermansia* was higher in patients with aGVHD (20/30) than in individuals with non-aGVHD (21/52) (P = 0.038; Fig. 4C). Our study utilized a random forest model to assess aGVHD-associated bacteria, ultimately identifying *Akkermansia muciniphila* as a significant bacterium (Fig. 4D). *Akkermansia muciniphila* mitigates proinflammatory pathways, including IL6-mediated signaling [32], throsugh its a15:0-i15:0 PE derivate, which can modulate LPS-mediated immune responses [33]. Unexpectedly, *Akkermansia muciniphila* exacerbates colitis in germ-free Il10$^{-/-}$ mice. Analysis of samples obtained from patients with aGVHD revealed enrichment in *s. Akkermansia_muciniphila*, prompting a reconsideration of the potential role of *Akkermansia muciniphila* as a conditioned pathogen contributing to an exaggerated immune response in the context of aGVHD (Supplementary Figure 4B). This suggests that alterations in gut microbiome composition may play a role in the development of aGVHD by impacting both innate and adaptive immune cells, thereby influencing the differentiation and function of T cells.

Hyperactivated αβ T cells impair immune homeostasis and type I IFN signaling in re-educated T cells mitigated against aGVHD

The microbiota and its metabolites control T cell responses; therefore, we analyzed the changes in T cells (Fig. 5A). Subsequently, differences in T subset composition between samples were evaluated, revealing elevated frequencies of αβ T cells in patients with aGVHD and γδ T cells in patients with non-aGVHD (Fig. 5B). Microbiota-derived lipid antigens play a crucial role in the maintenance of γδ T cells [34]. The MHC-independent activation of γδ T cells may be advantageous in preventing GVHD [35], and their antimicrobial functions are well established. Subsequently, we conducted GO and KEGG analysis on the upregulated DEGs in αβ T cells encompassing activated CD4$^+$ T, naïve T, proliferating CD8$^+$ T, effector CD8$^+$ T, proliferating CD4$^+$ T, and IFN response T subsets (IFN T subsets), derived from patients with aGVHD (Supplementary Figure 5A). Our analysis revealed that these genes were significantly enriched in pathways related to Th17 cell differentiation, and T cell regulation and activation (Fig. 5C). Furthermore, to ascertain T cell states, we investigated the levels of T cell-associated cytokines and observed elevated IL17A and IL4 levels in patients with aGVHD compared to those with non-aGVHD (Fig. 5D). Differential gene expression analysis in patients with aGVHD and non-aGVHD in various T cell subsets revealed several key genes implicated in aGVHD-related T cell function, including members of the AP-1 family (*FOS* and *JUN*), *IL32*, *TSC22D3*, *DUSP1*, *DUSP2*, *ZFP36L2*, *CD52*, *CD27*, *CD28*, and *GZMK* (Supplementary Figure 5B). GZMK was upregulated in patients with aGVHD (Fig. 5E), indicating its association with increased inflammatory T-cell function [36]. Conversely, the upregulated DEGs in αβ T cells from patients with non-aGVHD were enriched in pathways related to response to viral infection (Fig. 5F and Supplementary Figure 5C). The upregulation of Type I IFN-responded genes (MX1, STAT1, IFI44L, IFI6, IFITM2, and ISG15) in αβ T cells from patients with non-aGVHD, suggests that activated Type I IFN signaling may play a beneficial role in preventing aGVHD (Fig. 5G). Additionally, the upregulation of DEFA3 and KIR3DL2 in αβ T cells from patients with non-aGVHD is of interest. Notably, CD8$^+$ T cells expressing inhibitory killer cell immunoglobulin-like receptors (KIRs), such as including KIR3DL2, inhibit pathogenic CD4$^+$ T cells in autoimmune diseases and viral infections [37, 38]. Defensins, such as DEFA3, are a group of antimicrobial and cytotoxic peptides believed to play a role in host defense, suggesting that T cells from
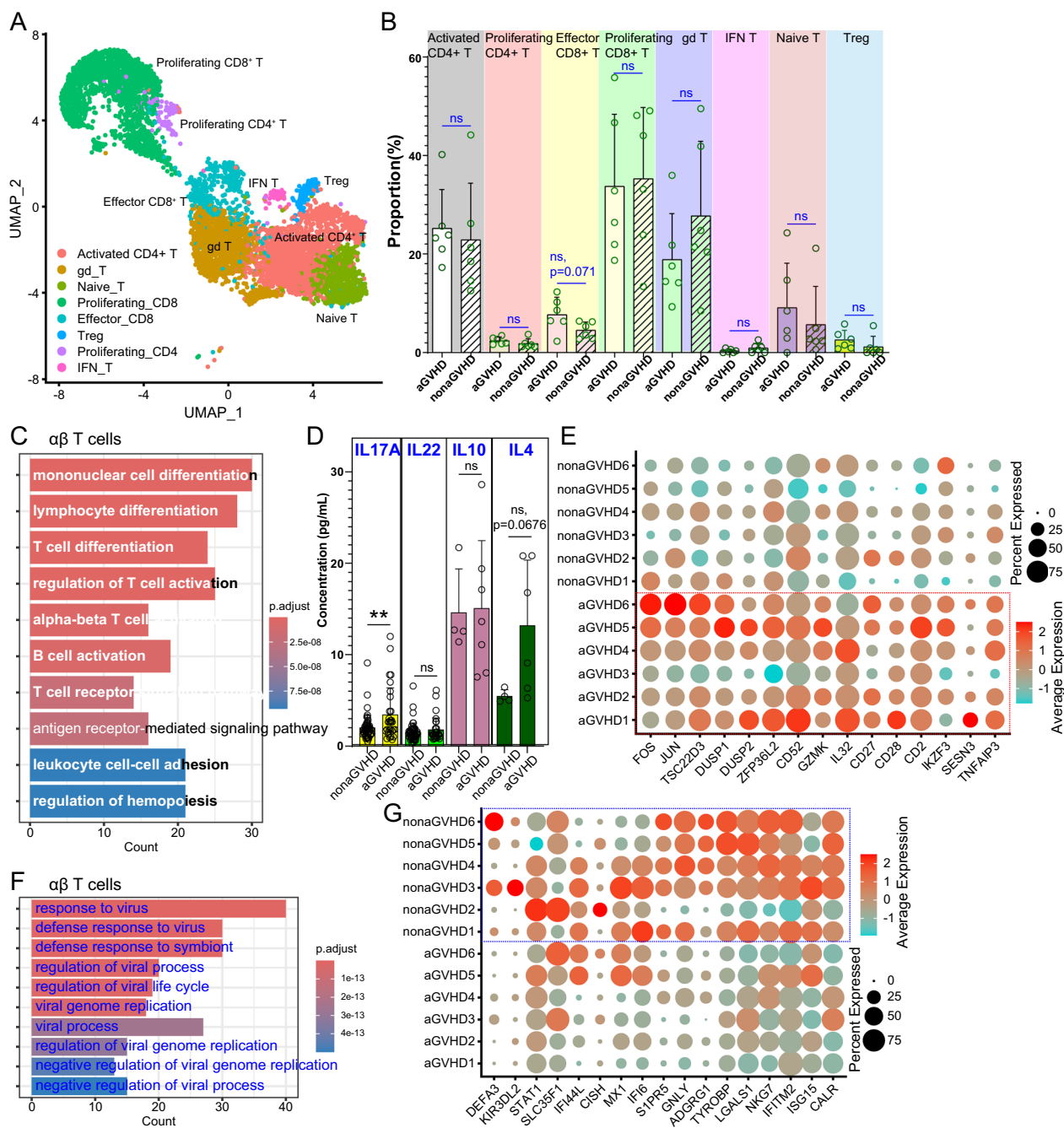
Han *et al. Journal of Translational Medicine*   (2024) 22:746

Page 10 of 24

Fig. 5 Distinguishing characteristic of T cells in patients with aGVHD. **A** UMAP visualization of scRNA-seq data of T cells from patients with aGVHD and individuals with non-aGVHD, with main cell subtypes annotated. **B** The frequency percentage of the main T cell subtypes. **C** Dot graph illustrating the GO analysis of upregulated genes in αβ T cells (including proliferating CD8^{+} T, proliferating CD4^{+} T, effector CD8^{+} T, IFN T, activated CD4^{+} T, and naïve T cells) from patients with aGVHD compared to those from individuals with non-aGVHD. **D** The levels of IL17A (patients with non-aGVHD, n = 52; patients with aGVHD, n = 30), IL22 (patients with non-aGVHD, n = 52; patients with aGVHD, n = 30), IL10 (patients with non-aGVHD, n = 4; patients with aGVHD, n = 7), and IL4 (patients with non-aGVHD, n = 4; patients with aGVHD, n = 6) in plasma samples from patients with aGVHD and individuals with non-aGVHD were measured using ELISA. **E** Dot plots were used to display the relative expression levels of upregulated genes (*FOS, JUN, TSC22D3, DUSP1, DUSP2, ZFP36L2, CD52, GZMK, IL32, CD27, CD28, CD2, IKZF3, SESN3,* and *TNFAIP3*) in αβ T cells from patients with aGVHD. **F** Dot graph illustrating the GO analysis of downregulated genes in αβ T cells from patients with aGVHD compared with those from individuals without aGVHD. **G** Dot plots were utilized to display the relative expression levels of downregulated genes (*DEFA3, KIR3DL2, STAT1, SLC35F1, IFI44L, CISH, MX1, IFI6, S1PR5, GNLY, ADGRG1, TYROBP, LGALS1, NKG7, IFITM2, ISG15,* and *CALR*) in PBMCs obtained from patients diagnosed with aGVHD

Han *et al. Journal of Translational Medicine*   (2024) 22:746

Page 11 of 24

individuals with non-aGVHD possess potent antibacterial capacities. Our research indicates a significant correlation between interferon (IFN)-responsive signaling and aGVHD prevention. Additionally, the ratio of αβ/γδ T cells is linked to aGVHD.

Immune cell-derived defensins limit infection and further inflammation via intestinal bacteria-regulated bile acid metabolism

Motivated by the increased expression of DEFA3 in T cells, we recognized the significance of defensins in aGVHD progression. Consistent with previous findings, both human and murine aGVHD are characterized by a deficiency in intestinal β-defensin induction, which has been linked to intestinal bacterial colonization [39]. We first aimed to understand whether defensin production was dysregulated in the PBMCs of patients with

aGVHD. Our analysis revealed that the expression levels of DEFB1, DEFA4, and DEFA3 were lower in PBMCs of patients with aGVHD than in those with non-aGVHD (Fig. 6A). We then analyzed the expression of these genes in lineages and found that DEFA3 was widely upregulated in all lineages in patients with non-aGVHD compared with that in individuals with aGVHD (Supplementary Figure 6A). In contrast, DEFA4 expression was predominantly limited to the granulocyte-like subset in patients with non-aGVHD (Fig. 6B). The production of defensins is influenced by bile acid metabolism [40].

To investigate the association between cholic acid metabolism and aGVHD, metabolomic analysis of bile acids in stool samples from patients undergoing allo-HSCT was conducted (Supplementary Figure 6B), resulting in the identification of two distinct sets of differential ingredients (Supplementary Figure 6C). Compared with
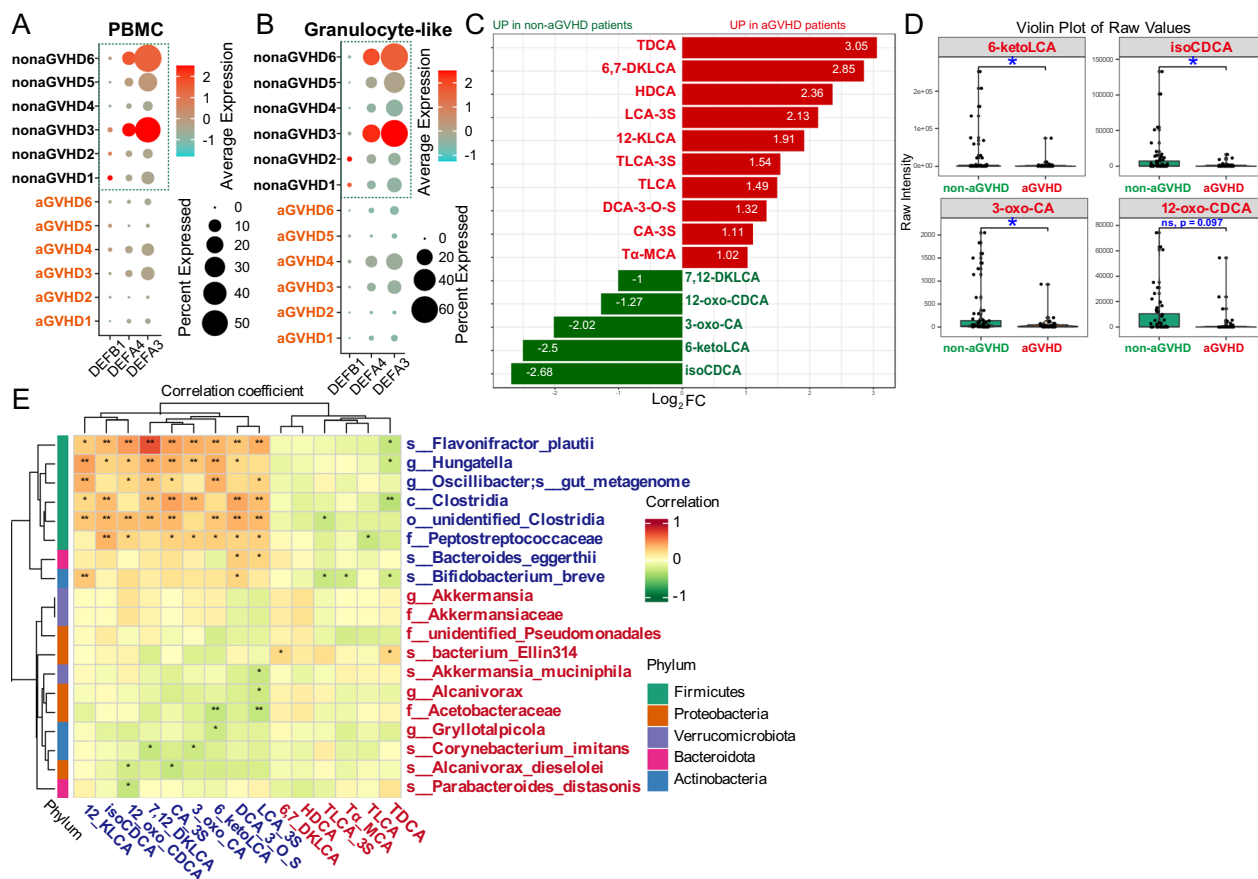

Fig. 6 Correlation between gut microbes and bile acid metabolism. **A** Dot plots were utilized to display the relative expression levels of *DEFB1*, *DEFA4*, and *DEFA3* in PBMCs obtained from patients with aGVHD and control individuals with non-aGVHD. **B** Dot plots illustrating the relative expression levels of *DEFB1*, *DEFA4*, and *DEFA3* in granulocyte-like cells derived from patients with aGVHD compared with those from individuals with non-aGVHD. **C** The metabolites exhibiting the greatest differential expression are ranked based on their $\log_2$ fold change ($\log_2$ FC) values. **D** Violin plots depicting the distribution of common bile acid metabolites within each group (patients with non-aGVHD, n = 52; patients with aGVHD, n = 30). **E** The relationship between bile acid metabolites and gut microbiota is examined through Spearman's correlation coefficients. Positive correlations are denoted by red fields, while negative correlations are denoted by green fields. Statistical significance is indicated by *P < 0.05, with **denoting significance after Bonferroni correction (P < 0.01)

Han *et al. Journal of Translational Medicine*   (2024) 22:746

Page 12 of 24

the aGVHD group, the non-aGVHD group exhibited a significant increase in the levels of isoCDCA, 6-ketoLCA and 3-oxo-CA (P=0.019, 0.035, and 0.015, respectively) (Fig. 6C, D). Moreover, differences in other bile acid metabolites between the aGVHD and non-aGVHD groups, such as 12-oxo-CDCA, TDCA, 6,7-DKLCA, HDCA, LCA-3S, DCA-3-O-S, CA-3S, 3β-UDCA and 7,12-DKLCA were observed, although these differences were not statistically significant (all P > 0.05) (Supplementary Figure 6D). The concentrations of isoCDCA, 6-ketoLCA, 3-oxo-CA, 12-oxo-CDCA, and 7,12-DKLCA were higher in the samples from patients with non-aGVHD than in those of patients with aGVHD. This observation is consistent with the known role of CDCA as a positive regulator of defensins [40, 41], as evidenced by the upregulated expression of defensins in patients with non-aGVHD. Additionally, taurodeoxycholic acid (TDCA) induces gastric inflammation by activating the IL-6/JAK1/STAT3 pathway in gastric epithelial cells [42]. TDCA activates hepatic stellate cells, thereby contributing to liver fibrogenesis [43]. Hyodeoxycholic acid (HDCA) can activate fatty acid oxidation in a PPARα-dependent manner [44]. Lithocholic acid 3-sulfate (LCA-3-S) is speculated to play a role in T lymphocyte differentiation [45], whereas 12-ketolithocholic acid (12-KLCA) may inhibit IL17A secretion from group 3 innate lymphoid cells (ILC3) [46]. Taurolithocholic acid 3-sulfate (TLCA-3S) induces inflammation [47], and taurolithocholic acid (TLCA) is implicated in immune regulation [48]. A negative correlation was observed between 6-ketoLCA and the serum levels of certain inflammatory cytokines in patients diagnosed with inflammatory bowel disease [49]. These results imply a potential association between cholic acid derivatives and aGVHD progression.

Moreover, intestinal bacteria play a role in bile acid metabolism, which is crucial for immune cell regulation [50]. The abundances of isoCDCA, 3-oxo-CA, and 6-ketoLCA exhibited significant positive correlations with the microbiota composition of *f_Peptostreptococcaceae*, *s_Flavonifractor_plautii*, and *g_Hungatella* within the *f_Lachnospiraceae* (r=0.38, 0.34, 0.24; P < 0.001, 0.002, 0.030; r=0.26, 0.40, 0.30, P=0.018, < 0.001, 0.005; r=0.27, 0.36, 0.39, P=0.012, < 0.001, < 0.001, respectively). These microbial taxa were all affiliated with the Firmicutes phylum, Clostridia class. Furthermore, 12-oxo-CDCA abundance displayed significant positive correlations with the abundance of *o_Clostridia*, *s_Flavonifractor_plautii*, *f_Peptostreptococcaceae*, *g_Hungatella*, and *g_Oscillibacter* (r=0.34, 0.46, 0.24, 0.28, and 0.23; P=0.002, < 0.001, 0.031, 0.010, and 0.041, respectively) (Fig. 5E). Our observations indicated a significant positive correlation between the abundance of TDCA, 6,7-DKLCA, and *s_bacterium_Ellin314* of

the *Proteobacteria phylum* (r=0.24, 0.22; P=0.032, 0.046, respectively). Additionally, the abundance of TDCA is negatively correlated with the abundance of *c_Clostridia*, *s_Bifidobacterium_breve*, *g_Hungatella* and *s_Flavonifractor_plautii* (r=−0.32, −0.23, −0.25, and −0.28; P=0.003, 0.040, 0.024, and 0.011, respectively) (Supplementary Figure 6E). The correlation coefficient demonstrated a relationship between bile acid metabolism and intestinal bacteria, with Firmicutes-mediated bile acid metabolism potentially offering protection against aGVHD following allo-HSCT. Conversely, *Proteobacteria*, *Verrucomicrobiota*, and *Actinobacteria* did not show the same correlation (Fig. 6E). As Bacteroides are significant source of bile salt hydrolase (BSH), we analyzed the prevalence of Bacteriodes. Our investigation revealed a decrease in Bacteriodes levels in samples obtained from patients with aGVHD compared with those from individuals with non-aGVHD, providing further evidence of compromised bile acid metabolism in patients with aGVHD (Supplementary Figure 6F).

Bile acid metabolites regulate immune responses by repressing the expression of S100A8/9/12 in CD16$^+$CD4$^-$ monocytes and macrophages

Bile acid metabolites directly modulate immune responses, prompting the investigation of the expression patterns of their receptors. Our analysis revealed that *GPBAR1* (TGR5) and *NR1H2* (LXRB) were predominantly expressed in the myeloid cell lineages, specifically in monocytes and DC (Supplementary Figure 7A). Interestingly, the expression levels of *GPBAR1* in the myeloid cell subset of almost all patients with aGVHD (4/6) were lower than those in individuals with non-aGVHD (Supplementary Figure 7B). Furthermore, we subdivided myeloid cells into smaller subsets (Supplementary Figure 7C, D) and investigated their differentiation processes (Supplementary Figure 7E). Interestingly, GPBAR1- and NR1H2-expressing cells were observed in a more differentiated cell population. Subsequently, DEGs in various myeloid subsets were analyzed based on the expression levels of *NR1H2* and *GPBAR1*. This analysis revealed the downregulation of certain proinflammatory genes (such as *CD74*, *ANXA2*, *FOS*, *IL17RA*, *S100A10*, and *HLA* genes) in GPBAR1- or NR1H2-expressing cells (Supplementary Figure 7G, H). Further investigations focused specifically on CD16$^+$CD14$^-$ monocytes and macrophage-like cells with high levels of GPBAR1 and NR1H2 expression, comparing DEGs based on the expression of these two receptors. GPBAR1- and NR1H2-expressing macrophage-like cells expressed S100A families at low levels (*S100A12*, *S100A8*, and *S100A9* in GPBAR1^{high} macrophage-like cells, and *S100A8* and *S100A9* in NR1H2^{high} subset) (Fig. 7A).

GPBAR1 and NR1H2-expressing CD14⁻CD16⁺ monocytes displayed low levels of S100A family expression (*S100A8* and *S100A9* in GPBAR1^high macrophage-like cells, and *S100A12*, *S100A8*, and *S100A9* in NR1H2^high subset) (Fig. 7B). Granulocyte-like cells were analyzed for DEGs based on *GPBAR1* and *NR1H2* expression. This analysis revealed that the expression of *GPBAR1* and *NR1H2* is involved in immunosuppression through the downregulation of S100A families and upregulation of leukocyte immunoglobulin-like receptor (LILR) family members (Supplementary Figure 7I–K). S100A family members are known drivers of inflammation, as they interact with receptors, such as RAGE, TLR4, CD36, and GPCR. Multiplex immunofluorescence of the small intestine revealed that CD45⁺ immune cells from the aGVHD mouse model showed increased S100A9 protein expression in the aGVHD mouse model compared with the non-aGHVD group (Fig. 7C). Our findings suggest a potential model of bile acid metabolite-mediated immune regulation involving the S100A family members in patients with aGVHD (Fig. 7D).

Distinct immune states in healthy donors, and patients with aGVHD and non-aGVHD

We compared the immune status of PBMCs from healthy donors (n = 4), and patients with aGVHD and non-aGVHD (Fig. 8A). Interestingly, we found that PBMCs from patients lacked the B/Plasma/pDC subset compared with those from healthy donors. Only granulocyte-like subsets were presented in these patients. The gene expression patterns in PBMCs from healthy donors and patients were distinct (Fig. 8B). Like PBMCs from patients with aGVHD, samples from healthy donors expressed IL1B, JUNB, FOS, JUN, and EGR1 at high levels, and IRF1, NLRC4, LILRB4, IRF7, LILRB1, and LILRB2 at low levels, compared with those from non-aGVHD patients. PBMCs of patients with aGVHD and non-aGVHD, showed a low expression of IL1R1 and IL1RAP. High expression levels of DEFA4 and DEFA3 are hallmark features of PBMCs from patients with non-aGVHD compared with those from healthy donors and patients with aGVHD. We assessed the expression levels of several genes in BM cells and splenic cells of mouse models of aGVHD using qPCR and identified different immune regulatory patterns in non-HCT, non-aGVHD,

and aGVHD groups (Fig. 8C and Supplementary Figure 8). Importantly, PBMCs of patients with non-aGVHD and healthy donors expressed at high levels of GPBAR1 and NR1H2, but not the PBMCs of patients with aGVHD, highlighting that bile acid metabolites are critical for immune homeostasis.

Discussion

scRNA-seq has facilitated the identification of intrinsic cell subsets that may play a role in cell fate determination and pathological functions at the single-cell levels [37, 51–54]. This technology has been used to investigate the molecular role of various hematopoietic and immune cell lineages in GVHD, including immune cells from gastrointestinal biopsies [55], T cells [56], skin-resident T cells [57], skin macrophages [58], invariant natural killer T cells from thymus [59], CD8⁺ T cells [60], and PBMCs [61]. CD8⁺ T cells are significant effectors and contributors to GVHD. Furthermore, reactive CD8⁺ T cells can potentially differentiate into inflammatory CD4/CD8 double-positive T cells, thereby playing a role in GVHD development [62]. Additionally, a study has shown that ex vivo-induced CD8^hi Tregs can effectively mitigate against GVHD by suppressing alloreactive T-cell proliferation[63]. Numerous novel T cell subsets are involved in GVHD, including CD3⁺CD4⁻CD8⁻ T [64], CD38^brightCD8⁺ T [65], and IL-17–producing CD8⁺ T cells [66]. The findings of our study demonstrated the upregulation of JUN in T cells derived from patients with aGVHD, suggesting a potential mechanism by which these T cells evade exhaustion by outcompeting exhaustion-inducing immunoregulatory transcription factors [67]. Furthermore, the interaction between JUN and FOS is essential for the T-cell effector function [68]. Additionally, Tsc22d3 has been identified as an inhibitor of the type I IFN response in DC [69], which is upregulated in T cells of individuals with aGVHD. Tsc22d3 can be induced by glucocorticoids and social-defeat stimuli, leading to the inhibition of FoxO3 transcriptional activity and subsequent protection of T cells from apoptosis [70]. This suggests that Tsc22d3 is a potential target for controlling aGVHD. Additionally, the upregulation of DUSP1 is essential for T cell activation and function [71]. Interestingly, DUSP2 is a negative regulator of TH17 [72], and is upregulated in T cells of patients with aGVHD.

(See figure on next page.)
Fig. 7 Relationship between *GPBAR1/NR1H2* expression and immune regulation in myeloid lineages through correlation analysis. **A** Volcano plots depicting the upregulated and downregulated DEGs in *GPBAR1* and *NR1H2*-expressing macrophage-like cells in comparison to their respective controls. **B** Volcano plots illustrating the upregulated and downregulated DEGs in *GPBAR1* and *NR1H2*-expressing CD14⁻CD16⁺ monocytes compared to their respective controls. **C** Representative immunofluorescence staining of CD45 and S100A9 in the small intestine of control or aGVHD mouse model groups. Scale bar, 50 μm. **D** Relevance of GPBAR1/NR1H2 in immune regulation
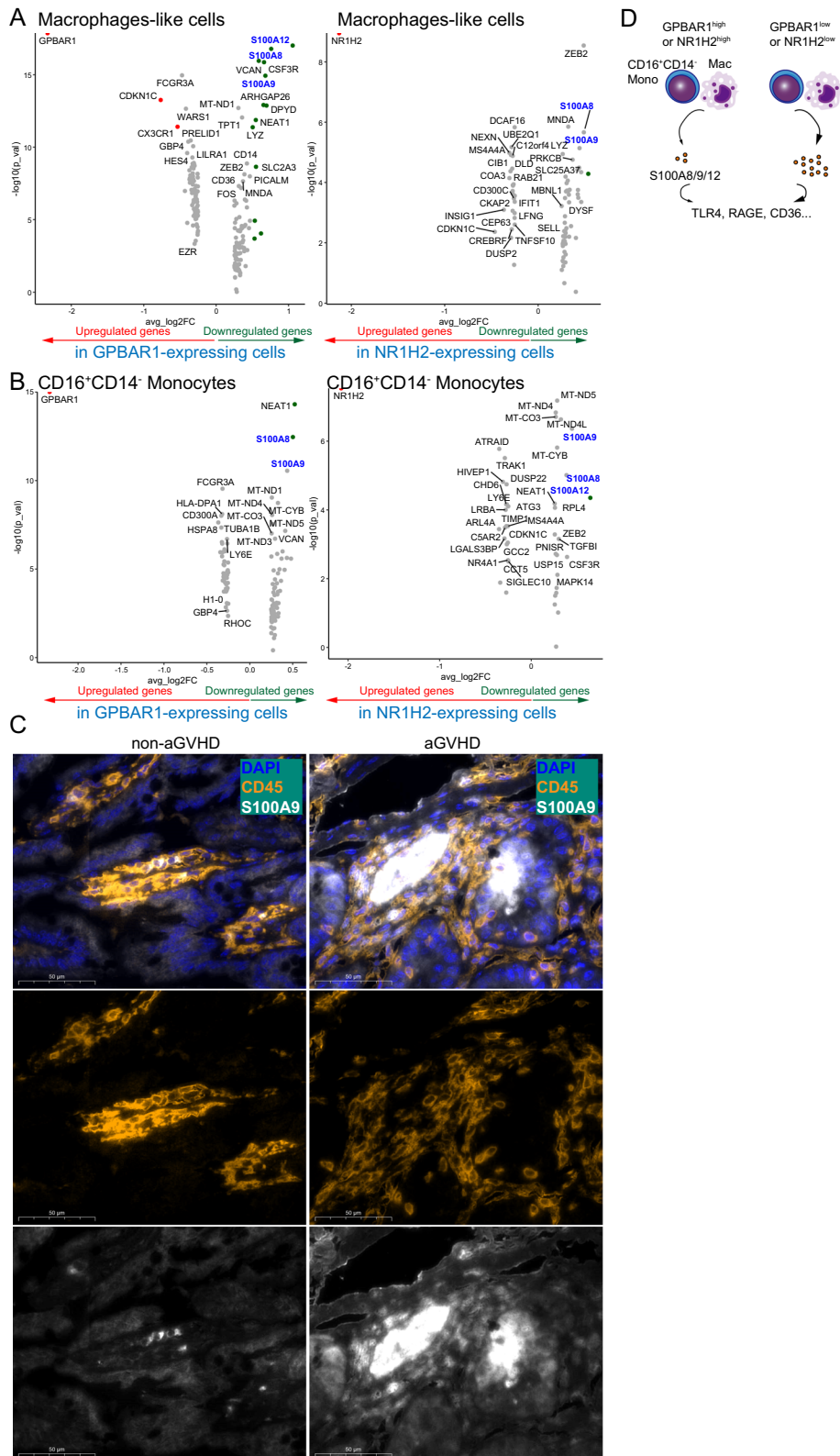
Fig. 7 (See legend on previous page.)

Han *et al. Journal of Translational Medicine*   (2024) 22:746
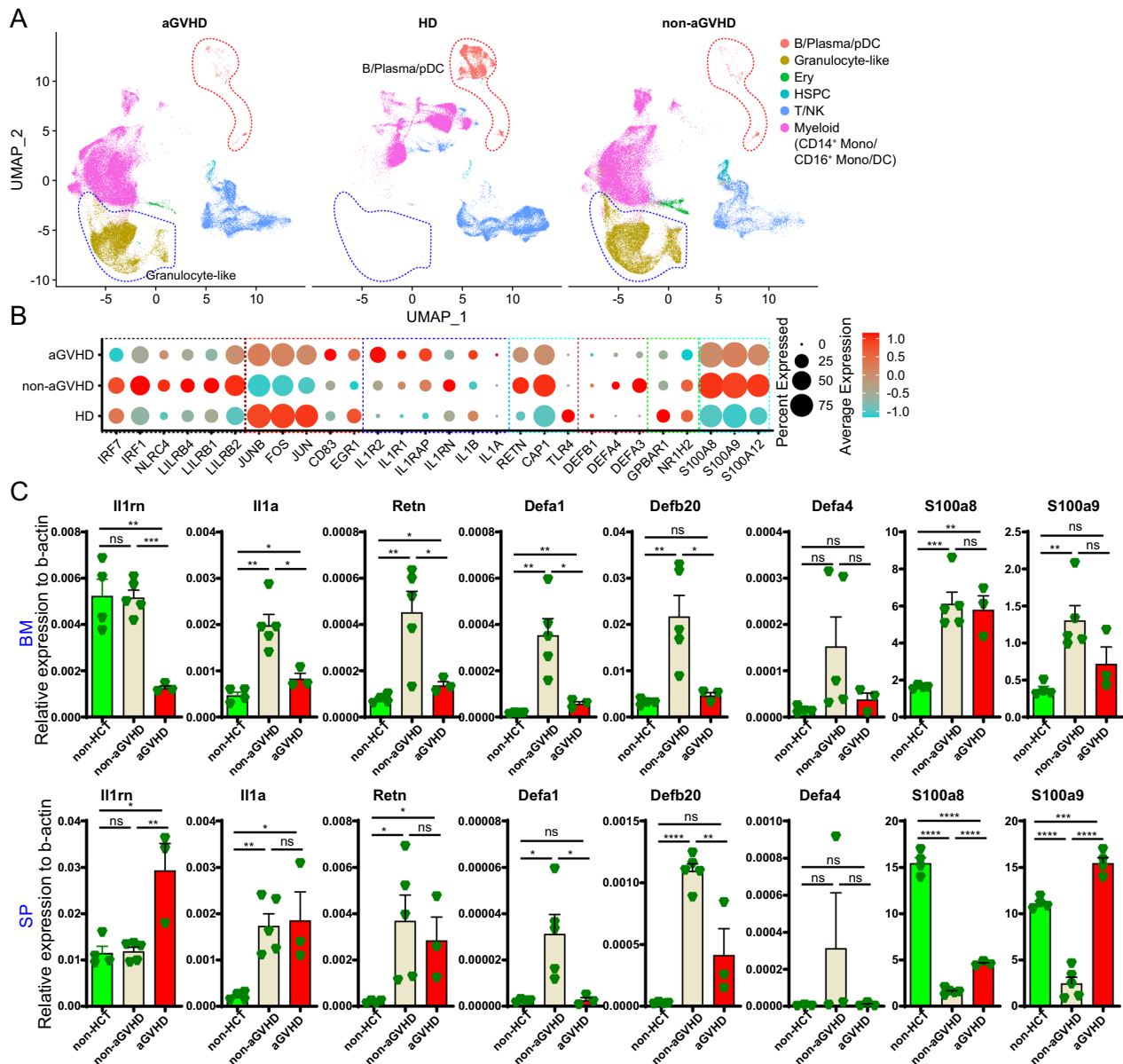
Page 15 of 24

Fig. 8 Immune states in patients with non-aGVHD differ from those in healthy donors and patients with aGVHD. **A** UMAP plot of scRNA-seq data from PBMCs of healthy donors, patients with aGVHD and with non-aGVHD, with cell subtypes labeled. **B** Dot plots illustrating relative expression levels of selected genes in PBMCs obtained from healthy donors, patients with aGVHD, and patients with non-aGVHD. **C** mRNA expression levels of selected genes in bone marrow cells and splenic cells from control groups, mice with BM transplantation, and mice with aGVHD (day 4)

Other upregulated genes, such as GZMK, CD27, CD28, and IL32, indicated an activated state of T cells in individuals with aGVHD.

The upregulated expression of KIR3DL2, CISH, LGALS1, and genes associated with the type I IFN pathway (STAT1, IFI44L, IFI6, and MX1) in T cells of patients with non-aGVHD suggests the utilization of key signaling pathways for the re-establishment of immune homeostasis. CD8$^+$ T cells expressing inhibitory killer cell

immunoglobulin-like receptors (KIRs) may play a role in suppressing pathogenic CD4$^+$ T cells [38], indicating the potential involvement of KIR$^+$CD8$^+$ Tregs in inhibiting alloimmune responses in individuals with non-aGVHD. STAT1 is essential for type I and II IFN receptor signaling, and its absence in naïve CD8$^+$ T cells resulted in severe colonic inflammation in a mouse model of inflammatory bowel disease due to the activation of the type I IFN-STAT4-mTORC1 signaling pathway [73]. IFI44L is

Han *et al. Journal of Translational Medicine*　　(2024) 22:746

Page 16 of 24

a negative regulator of IFN-mediated proinflammatory responses [74]. CISH function as an intracellular immune checkpoint that inhibits T cell activation, and its deficiency can lead to T cell hyperactivation [75]. S1PR5 regulates immune cell trafficking and is involved in GVHD pathogenesis [76]. ADGRG1 (GPR56) may potentially mitigate the cytotoxic effects of cytotoxic T cells [77]. These results indicate that the transcriptional state of T cells in individuals with non-aGVHD may be characterized by a type I IFN response. Unlike other similar studies, we not only investigated abnormal T-cell immunity but also focused on resolving the crosstalk between innate immunity and microorganisms and their metabolites [56, 58, 60, 61, 78].

Type I IFNs play a dual role in the immune response by promoting inflammation against pathogens and maintaining immune tolerance in the gut through APC-Treg communication without the production of IL-1β and IL17A [79]. This regulatory mechanism is contingent on the presence of commensal bacteria [80]. Impaired type I IFN-dependent responses are associated with poor disease outcomes in patients with severe SARS-CoV-2 infection [81]. Type I interferon-alpha2a does not exacerbate aGVHD [82]. IFN-α treatment decreases the levels of pro-IL1α/β and inhibits the secretion of mature IL-1β in human monocytes [83]. Activation of NLRP3 in myeloid cells enhances immune responses by releasing bioactive IL-1β [84]. The recruited monocytes play a crucial role in the production of IL-1β during intestinal inflammation induced by commensal bacteria, and the microbiota composition influences the bacteria-induced production of IL-1β [85]. Our findings indicate that IL1B is upregulated in myeloid cells of patients with aGVHD, leading to the activation of the IL-1β-related signaling pathway and suggesting a potential role for intestinal microbiota composition in the pathogenesis of aGVHD. Additionally, our study revealed decreased expression levels of RETN and defensin genes in the cells of individuals with aGVHD compared with those of patients with non-aGVHD. Resistin encoded by RETN, and defensins play crucial roles in the antimicrobial innate immune response [86, 87]. α-Defensins can selectively eliminate noncommensal microorganisms while preserving commensal ones, a phenomenon closely linked to GVHD but not to conditioning-induced intestinal injury [87]. These findings suggest that alterations in intestinal microbiota composition in the context of GVHD are associated with antimicrobial efficacy and the upregulation of IL-1β-mediated inflammatory signaling. Consequently, resistin, defensins, and IL-1β may represent promising targets for aGVHD.

The intestinal microbiota composition and its metabolic byproducts play a significant role in the GVHD regulation [11]. Akkermansia species, known for their mucus-degrading capabilities, have been implicated in the impairment of the intestinal barrier, thereby contributing to the development of GVHD [88]. Conversely, a decrease in *Clostridiales* abundance was consistently observed in patients with aGVHD, a finding corroborated by a previous study [89]. *Clostridiales* has been shown to modulate immune responses through its involvement in bile acid metabolism [10]. *Peptostreptococcaceae* may also play roles in immune regulation and surveillance [90]. Bifidobacterium breve facilitates bile acid deconjugation within the intestinal tract and inhibits inflammatory reactions [91]. Additionally, *Flavonifractor plautii* may play a role in bile acid metabolism [92], whereas *Hungatella* has been implicated in bile acid metabolism and has shown to have a negative correlation with CD8^{+} T cell infiltration [93, 94]. These findings indicate that the composition of the intestinal microbiota may modulate immune balance through bile acid metabolism [88], offering the potential for the development of a promising anti-aGVHD therapy.

This study has some limitations. First, our results need to be supported by additional experiments using animal models. Secondly, it was impossible to rule out interference from other essential treatments. Finally, many genes and stimulators, such as resistin, are pleiotropic at the cellular and animal levels, and it is difficult to obtain a perfect regulatory network for these potential factors in aGVHD pathogenesis. However, our study presents direct evidence of the key factors involved in aGVHD progression, rather than vague and forced speculation. First, we highlighted two sets of genes used to predict aGVHD: one set of genes (JUNB, FOS, JUN, CD83, and EGR1) was upregulated in the aGVHD group and one set of genes (IRF7, IRF1, NLRC4, LILRB4, LILRB1, and LILRB2) was downregulated in the aGVHD group. Second, our work provides unequivocal evidence for the role of the IL1B-triggered signaling pathway in aGVHD, and markedly illustrates the interaction between DAMPs/PAMPs, IL1B, and resistin. Finally, our analysis of fecal microbiota and bile acid metabolism provides novel insights into targeting imbalanced gut flora and bile acid metabolites.

Conclusion

Our study revealed that hyperactivated immune responses in aGVHD are exacerbated by alterations in the intestinal microbiota composition and impaired bile acid metabolism (Fig. 9). The uncontrolled signaling of IL-1β is a prominent feature of aGVHD, which suggests that drugs targeting IL-1β, such as anakinra, rilonacept, and canakinumab, are potential therapeutic options. Importantly, we found that the expression patterns of
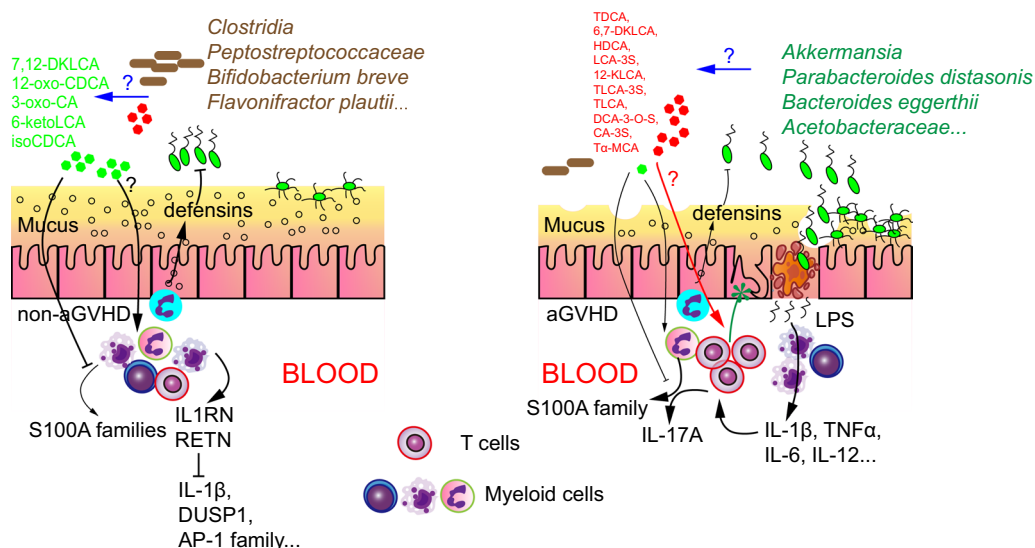
Fig. 9 A simplified schematic diagram illustrating the dysregulated gut microbiota and bile acid metabolism positive feedback loop, which exacerbates immune responses and exacerbates aGVHD. Improper treatment of patients undergoing allo-HSCT alters the gut microbiota and disrupts the imbalanced bile acid metabolism. Dysregulated bile acid metabolism results in reduced production of IL1RN, defensins, and resistin. Deficiency of defensins and resistin fails to inhibit harmful microorganisms, leading to increased production of proinflammatory cytokines and proteins, such as IL-17A, IL-1β, TNFα, IL-6, IL-12, and members of the S100A family. Additionally, it was determined that resistin can inhibit aGVHD by downregulating the expression of IL1B, DUSP1, and members of the AP-1 family

resistin and defensins were abnormal, indicating that weakened antimicrobial ability in non-aGVHD patients is a probable driver of amplified proinflammatory. Strategies, such as modulating the microbiota, restoring bile acid metabolism, targeting IL-1β signaling, and utilizing peptides derived from resistin or defensins show promise as effective approaches for treating aGVHD.

Methods

Study's aim, design, and setting

A cohort of 96 patients who underwent myeloablative allo-HSCT was enrolled at the First Affiliated Hospital of Zhengzhou University (ZZU) between February 2023 and November 2023 (Supplementary Figure 9). At 15 ± 1 days post-transplantation, samples were obtained from the recipients (Supplementary Table 1). Fourteen patients, of which one died before the engraftment, 12 had insufficient fecal or blood samples, and one patient underwent donor lymphocyte infusion (DLI) due to hematologic relapse within 100 days post-transplantation, were excluded from the study. The final cohort consisted of 82 patients, with 30 patients experiencing grade II–IV aGVHD (aGVHD group) and 52 patients without aGVHD (non-aGVHD group) within 100 days post-transplantation. This study was approved by the Ethical Committee of First Affiliated Hospital of Zhengzhou University and the participants provided consent by providing a signature for the collection and analysis of

biospecimens. The study adhered to the guidelines outlined in the Declaration of Helsinki.

Characteristics of the patients

The study cohort consisted of 59 males and 23 females, with a median age of 33 years (range: 14–59 years) (Supplementary Figure 8). The primary diseases included acute myeloid leukemia, acute lymphoblastic leukemia, myelodysplastic syndrome, and severe aplastic anemia. Overall, 27 patients received HLA-matched sibling donor transplant, 47 received a haploidentical donor transplant, and eight received an HLA-matched unrelated donor transplant. There were no discernible disparities in antibiotic usage (carbapenem and vancomycin) between the two groups. Most patients received naturally sourced nutrients during sampling, thereby mitigating against the potential effects of enteral or artificial parenteral nutrition.

Collection of fecal samples and analysis of bile acid metabolites

Fecal and blood specimens were obtained from the patients on post-transplantation day 15 ± 1. These samples were labeled and preserved at −80 °C until analysis. Any samples not promptly preserved within 6 h of collection were excluded from the study.

Fecal samples were treated using a ball mill, and 20 mg was subjected to an extraction process with 200 μL of

Han *et al. Journal of Translational Medicine*   (2024) 22:746

Page 18 of 24

methanol. A 10 µL solution containing internal standards at a concentration of 1 µg/mL was added to the extract for quantification purposes. The samples were then subjected to protein precipitation at -20 °C for 10 min and centrifuged for 10 min at 12,000 r/min and 4 °C. Subsequently, the supernatant was collected and analyzed using a LC–ESI–MS/MS system (UHPLC, ExionLC™ AD, https://sciex.com.cn/; MS, Applied Biosystems 6500 Triple Quadrupole, https://sciex.com.cn/). The analytical conditions of the HPLC analysis were: column, Waters ACQUITY UPLC HSS T3 C18 (100 mm×2.1 mm i.d., 1.8 µm); solvent system, water with 0.01% acetic acid and 5 mmol/L ammonium acetate (A), acetonitrile with 0.01% acetic acid (B); a gradient elution program starting at 5–40% of B in 0.5 min, further increasing to 50% of B in 4 min, then to 75% of B in 3 min, and then 75–95% in 2.5 min, washed with 95% of B for 2 min, finally ramped back to 5% of B (12–14 min); a flow rate of 0.35 mL/min; a temperature of 40 °C; and injection volume of 1 µL. The effluent was connected to an ESI-triple quadrupole-linear ion trap (QTRAP)-MS system for analysis. Bile acids were analyzed using scheduled multiple reaction monitoring (MRM) on a QTRAP 6500 + LC–MS/MS System, operating in negative ion mode and controlled by Analyst 1.6.3 software (Sciex). Data were acquired using the same software. The multiquant 3.0.3 software (Sciex) was used to quantify all metabolites. Mass spectrometer parameters, such as the declustering potentials (DP) and collision energy (CE), for individual MRM transitions were optimized by further adjusting the DP and CE values. A specific set of MRM transitions was monitored for each period based on the elution profiles of the metabolites. Differentially regulated metabolites between groups were identified using a combination of VIP scores and absolute Log2FC (fold change) values. VIP values were obtained via the OPLS-DA, which included score and permutation plots, using the R package MetaboAnalystR. Before OPLS-DA, the data underwent log transformation (log2) and mean centering. To prevent overfitting, a permutation test was conducted with 200 permutations.

16s rRNA gene sequencing
For 16s rRNA gene sequencing, DNA was extracted and analyzed as described previously [95]. DNA concentration and purity were assessed using 1% agarose gel. Depending on the concentration, DNA was diluted to 1 ng/µL using sterile water. Subsequently, sequencing libraries were constructed using a TruSeq DNA PCR-Free Sample Preparation Kit (Illumina) following the manufacturer's guidelines, and index codes were added. Library quality was evaluated using a Qubit 2.0 Fluorometer (Thermo Scientific) and an Agilent Bioanalyzer 2100 system. Finally, the library was sequenced using an Illumina NovaSeq platform. A nonparametric factorial Kruskal–Wallis rank-sum test was used to distinguish various microbiota taxa and identify significantly different and abundant features among the groups. Linear Discriminant Analysis Effect Size (LEfSe) was used to discern distinct characteristics between the groups. Random forest analysis was performed by extracting multiple samples from the original dataset using a bootstrap aggregation resampling method, followed by modeling the training set as a decision tree. The mean decrease accuracy was used to assess the degree of accuracy of the random forest analysis by changing the value of a variable to a random number. A higher value indicates a greater importance of the variable. The random forest model is implemented using the *varSelRF* package. To visually represent the correlations between microorganisms and metabolites, hierarchical clustering analysis based on Spearman's correlation was conducted on the differential microorganisms and metabolites. A correlation heatmap was generated using the Complex Heatmap package in R.

Clinical samples and scRNA-seq
Peripheral blood (PB) samples were obtained from six patients who underwent allo-HSCT, each from the aGVHD and non-aGVHD groups. PB samples were collected in EDTA anticoagulant tubes for the enrichment analysis of mononuclear cells (MNCs) using Ficoll-Paque PLUS (Cat# 17144003, Cytiva). The MNCs were adjusted to a concentration of 100,000 cells/mL using PBS before loading onto a microfluidic device. Libraries were prepared using a GEXSCOPE single-cell RNA-Library Kit (Cat# 5180012, Singleron) and sequenced using a DNB-seq T7 system (MGI Tech). Gene expression matrices were derived from raw reads using CeleScope V1.9.0 pipeline and Cutadapt v1.17. STAR v2.6.1a was used to map the reads to reference genome GRCh38, whereas feature-Counts v2.0.1 was utilized to generate expression matrix files.

Cell culture
THP-1 cells were cultured in in RPMI1640 medium (Cat# 41402ES76, YEASEN) in 10 cm dishes supplemented with 10% FBS (Cat# 40131ES76, YEASEN) and 1×P/S (Cat# 60162ES76, YEASEN). The cells were maintained at 37 °C in a 95% air and 5% CO_2 atmosphere for experiments after two passages. THP-1 cells were plated at a density of $1×10^6$ cells/mL in 24-well cell culture dishes, and the medium was replaced with RPMI1640 supplemented with 10% FBS, 1×P/S, and 100 ng PMA (Cat. No. S1819, Beyotime) for 24 h before experimentation. Following PMA stimulation, the culture medium was replaced with RPMI1640 supplemented with 10% FBS, 1×P/S, and LPS (1, 10, or 100 ng/mL) (Cat#

Han *et al. Journal of Translational Medicine*   (2024) 22:746

Page 19 of 24

L8880, Salarbio) or recombinant human resistin (1, 10, and 100 ng/mL) (Cat# CJ48, novoprotein) for 24 h. The resulting cell-free supernatants were harvested and centrifuged at 500×*g* for 10 min.

Cytokine detection

Cell-free supernatants were assessed using the Human IL1b (Interleukin 1 beta) ELISA Kit (Cat# ELK1270, ELK Biotechnology) according to the manufacturer's guidelines. The LPS, TNF-α and IL-22 concentrations in plasma samples were analyzed using Human LPS ELISA Kit (Cat# orb407527, biorbyt), Human TNF-alpha Quantikine ELISA Kit (Cat# DTA00D, R&D Systems), and Human IL-22 Quantikine ELISA Kit (Cat# D2200, R&D Systems), respectively. The concentrations of additional cytokines in plasma were assessed using an Immunology Multiplex Assay (HCYTOMAG-60K-06. Hum) following the manufacturer's guidelines.

scRNA-seq analysis of samples from patients with or without aGVHD

Dimension reduction, cell clustering, reclustering, and differential gene expression analyses were performed using the *Seurat* package. Cell communication analysis was performed using the *Cellchat* package, and GO/KEGG analysis was performed using the *ClusterProfiler* package. Pathway visualization was performed using the R package *pathview*. Differential gene expression analysis was carried out through the function "FindMarkers(object, ident.1 = ident.1, ident.2 = ident.2, method = "DESeq2")." Venn diagrams were constructed using R packages *vennDiagram* and *venn*. Cell clusters were identified based on marker gene expression, as outlined in Supplementary 1A (CD14$^+$ Monocytes: *VCAN*, *CD14*, *S100A8*, and *S100A9*; CD16$^+$ Monocytes: *FCGR3A*, *CSF1R*, *CX3CR1*, and *CKKN1C*; granulocyte-like subset: *FCGR3B*, *CEACAM8*, *CD177*, *ITGAX*, and *CSF3R*; T/NK subset: *CD3D*, *CD3E*, *CD3G*, *TRAC*, *NCAM1*, and *NKG7*; B/Plasma/pDC subset: *IL3RA*, *JCHAIN*, *CD19*, *MS4A1*, *IL4R*, *CD38*, *IGHD*, and *IGHM*; HSPC: *CD34*, *HOXA9*, and *FLT3*; Erythroid lineage: *HBA1*, *HBA2*, and *HBB*; and DC: *CD1C*, *HLA-DPB1*, *HLA-DPA1*, *HLA-DQA1*, *CD1E*, *FCER1A*, *CLEC10A*, and *FCGR2B*). Lineage-specific genes were used to identify *CD3D*, *CD3E*, and *CD3G*-expressing T subsets, including naïve T cells (*CCR7*, *TCF7*, *LEF1*, and *SELL*), γδ T cells (*TRDC*, *TRGC1*, and *TRGC2*), Treg (*CD4*, *IL2RA*, *FOXP3*, *CTLA4*, and *IKZF2*), IFN-response T cells (*IFIT3*, *ISG15*, *MX1*, and *IFI44L*), Proliferating CD4$^+$ T cells (*CD4*, *TYMS*, and *MKI67*), Proliferating CD8$^+$ T cells (*CD8A*, *CD8B*, *TYMS*, and *MKI67*), and effector CD8$^+$ T cells (*CD8A*, *CD8B*, *GNLY*, and *GZMB*), while activated CD4$^+$ T cells expressed low expression levels of naïve T markers and high expression levels of *RORA*, *IFNGR1*, *GATA3*, and *PDCD1*). The myeloid subsets were categorized into five clusters as outlined in Supplementary Figure 7C (CD14$^+$CD16$^-$ monocytes, CD14$^+$CD16$^+$ monocytes, CD14$^-$CD16$^+$ monocytes, *C1QA*, *C1QB*, and *C1QC*-expressing macrophage-like cells, and *CD1C* and *CD1E*-expressing DC subset). Granulocyte-like cells were reclustered into four subsets (TLR2$^+$ subset: *TLR2* and *ABCA1*; S100A$^+$ subset, *S100A6*, *S100A8*, *S100A9*, *S100A11*, and *S100A12*; ARG1$^+$ subset, *ARG1* and *RETN*; DEFA3$^+$ subset, *DEFA3*, *DEFA4*, *MKI67*, *TOP2A*, *MPO*, *ELANE*, and *CEACAM8*).

scRNA-seq analysis of LPS-treated PBMCs and resistin-treated immune cells

The scRNA-seq datasets of LPS-treated PBMCs and their control groups were obtained from EMBL-EBI (https://www.ebi.ac.uk/ena/browser/view/PRJEB40448), and analyzed using Seurat [96]. The scRNA-seq datasets of resistin-treated immune cells and control groups were downloaded from Immune Dictionary (https://www.immune-dictionary.org/app/home), and the differential gene expression analysis was carried out through the function "FindMarkers(object, ident.1 = ident.1, ident.2 = ident.2, method = "DESeq2")."

Mouse model of aGVHD

C57BL/6 and BALB/c mice, aged 8 to 12 weeks and weighing 25–30 g, were sourced from the Animal Experiment Center of Zhengzhou University to model aGVHD. The mice were maintained in a pathogen-free environment at the Animal Experiment Center of Zhengzhou University. All experimental procedures involving animals were conducted in accordance with the protocols approved by the Ethical Committee of Zhengzhou University. Bone marrow (BM) cells from wild-type C57BL/6 mice were isolated from the compact bones of the donors. The femurs and tibias were dissected to collect the BM cells, which were then washed with DPBS containing 10% FBS and isolated. The BALB/c recipients were irradiated at a dose of 700 cGy before HSCT. Recipients were then injected with either 5×10^6 donor BM cells alone (non-aGVHD group), 5×10^6 bone marrow cells with 3×10^6 splenocytes (aGVHD group), or 100 μL PBS (non-HCT group). The evaluation of GVHD encompassed the assessment of clinical symptoms, which were conducted as previously described with some adjustments [97, 98]. The scoring system for clinical symptoms of aGVHD included parameters such as weight loss, posture, activity, and diarrhea. Mice were monitored until the 14-day endpoint, at which point those exhibiting severe GVHD were euthanized. The tissues were harvested during necropsy, fixed in 10% buffered formalin, and embedded in

paraffin. Specific BM cells were isolated from the compact bones of the femur and tibia for further analysis.

Multiplex immunohistochemical staining in fluorescence

Formalin-fixed paraffin-embedded small intestine sections, sliced at a thickness of 5 μm, were mounted onto slides. Sections were deparaffinize using de-paraffin liquid (Cat# G1128, Servicebio) and dehydrated using an alcohol gradient. Subsequently, the sections were treated with antigen retrieval buffer (Cat# G1202-250ML, Servicebio) and 3% hydrogen peroxide at room temperature for 25 min in the dark. Subsequently, 3% BSA (Cat# GC305010, Servicebio) was applied to the slides, which were sealed and incubated at room temperature for 30 min. Subsequently, the slides were incubated with primary antibodies overnight at 4 °C, followed by three washes with PBS (pH 7.4) (Cat# G0002, Servicebio). The following primary antibodies were used: Anti-IRF7 Rabbit pAb (1:500, Cat# GB111169, Servicebio), Anti-c-Jun Rabbit pAb (1:500, Cat# GB11515, Servicebio), Anti-c-Fos Mouse mAb (1:1000, Cat# GB12069, Servicebio), Anti-CD45 Rabbit pAb (1:1000, Cat# GB113886, Servicebio), Anti-Resistin Rabbit pAb (1:5000, Cat# GB112526, Servicebio), and Anti-S100A9 Rabbit pAb (1:500, Cat# GB111149, Servicebio). The slides were incubated with secondary antibodies specific to the primary antibody species at room temperature for 50 min. The following secondary antibodies were used: HRP-labeled goat anti-rabbit IgG secondary antibody (1:500, Cat# GB23303, Servicebio), and HRP-goat anti-mouse secondary antibodies (1:500, Cat# GB23301, Servicebio). After washing the slides thrice with PBS, they were exposed to iF440-Tyramide (1:500, Cat. No. G1250, Servicebio), iF488-Tyramide (1:500, Cat. No. G1231, Servicebio), iF546-Tyramide (1:500, Cat. No. G1251, Servicebio), iF555-Tyramide (1:500, Cat. No. G1233, Servicebio), iF594-Tyramide (1:500, Cat. No. G1242, Servicebio), iF647-Tyramide (1:500, Cat. No. G1232, Servicebio), and iF700-Tyramide (1:500, Cat. No. G1252, Servicebio).

Reverse-transcription quantitative PCR

Mouse BM cells and splenic cells were treated with red blood cell lysis buffer (Cat# R1010, Solarbio). The samples were then treated with TRIzol reagent (Cat# 15596026, Invitrogen), and cDNA was synthesized using the HiScript II cDNA Reverse Transcriptase Kit (Cat# R223, Vazyme) with total RNA as the starting material. Gene expression analysis was performed using a Quant-Studio 3 instrument and SYBR reagent (Cat# 11202, Yeasen). The following primers were used: *β-actin*: forward (CATTGCTGACAGGATGCAGAAGG) and reverse (TGCTGGAAGGTGGACAGTGAGG); mouse *Ilr1*: forward (CTGTTGGTGAGGAATGTGGCTG) and reverse (GGCTCAGGATAACAGGTCTGTC), mouse *Ilr2*: forward (CAGTGCAGCAAGACTCTGGTAC) and reverse (GCAAGTAGGAGACATGAGGCAG), mouse *Il1rap*: forward (GGAGGATCTCAGGCGCAACTAT) and reverse (CCAGAAAGACCGTGGCTCCAAA), mouse *Il1rn*: forward (TGTGCCTGTCTTGTGCCAAGTC) and reverse (GCCTTTCTCAGAGCGGATGAAG), mouse *Il1b*: forward (TGGACCTTCCAGGATGAGGACA) and reverse (GTTCATCTCGGAGCCTGTAGTG), mouse *Il1a*: forward (ACGGCTGAGTTTCAGTGAGACC) and reverse (CACTCTGGTAGGTGTAAGGTGC), mouse *Retn*: forward (CATGCCACTGTGTCCCATCGAT) and reverse (ACTTCCCTCTGGAGGAGACTGT), mouse *Tlr4*: forward (AGCTTCTCCAATTTTTCAGAACTTC) and reverse (TGAGAGGTGGTGTAAGCCATGC), mouse *Cap1*: forward (TTGACTCGCTGCTTGCCAATCC) and reverse (CACTGAGAAGCTGTAGCCAGGA), mouse *Defb20*: forward (AAGGCTACTGTAGGAAGAAATGCA) and reverse (CAACGACTGAGTGCTTCTTGTGC), mouse *Defa1*: forward (AACTGAGGAGCAGCCAGGAGAA) and reverse (CTTCCTTTGCAGCCTCTTGATCT), mouse *Defa4*: forward (CTAATACTGAGGAGCAGCCAGG) and reverse (GCAGTGTCCTTTTCTACAATAGCA), mouse *S100a8*: forward (CAAGGAAATCACCATGCCCTCTA) and reverse (ACCATCGCAAGGAACTCCTCGA), mouse *S100a9*: forward (TGGTGGAAGCACAGTTGGCAAC) and reverse (CAGCATCATACACTCCTCAAAGC).

Supplementary Information

Supplementary Material 1: Supplementary Figure 1. Atlas of the immune cells of patients undergoing HSCT.. Dot plots showing the expression levels of lineage-specific marker genes.. Dot plots showing the expression levels of genes from the "immune response-regulating signaling pathway" geneset.. Bar plots displaying the KEGG analysis of upregulated genes in PBMCs from patients with non-aGVHD compared with those from individuals with aGVHD.. KEGG Pathview analysis displaying downregulated genes of "neutrophil extracellular trap formation" and "PHAGOSOME" pathways in patients with non-aGVHD.. Dot plots showing the expression levels of genes from the "mononuclear cell differentiation" geneset.. KEGG analysis of upregulated genes in PBMCs from patients with aGVHD compared with that from individuals with non-aGVHD.

Supplementary Material 2: Supplementary Figure 2. Disparity in cell communication through IL-1 signaling between patients with aGVHD and those with non-aGVHD.. Circular plots displaying both the quantity and intensity of inferred interactions.. Dot plot depicting the relative expression levels of IL-1 signaling-associated ligands and receptors in various immune cell subtypes, including PBMCs, DC, erythroid lineage, B/Plasma/pDC and T/NK subtypes within each sample.. Venn diagrams illustrating the shared upregulatedand downregulatedgenes in LPS-treated PBMCs and PBMCs derived from patients with aGVHD.. The protein level of IL-8 detected by ELISA assay.

Supplementary Material 3: Supplementary Figure 3.. Expression of RETN and its receptor CAP1 in PBMCs and other cell subtypesamong each sample.. Venn diagrams illustrating the shared conserved upregulated genes

Han *et al. Journal of Translational Medicine*   (2024) 22:746

Page 21 of 24

among distinct lineagesvs. B cells; group 4: CD4$^+$ T cells vs. CD8$^+$ T cells vs. Treg; group 5: innate lymphoid cellvs. γδ T cells vs. NK cells).

Supplementary Material 4: Supplementary Figure 4. Potentially detrimental alterations in gut bacteria population in patients with aGVHD.. Linear Discriminant Analysisscores were utilized to compare the differential abundance of species between individuals with aGVHDor with non-aGVHD. The LDA scores serve as a measure of the effect size for each abundant species. Species enriched in either group with an LDA score > 2 are deemed significant.. Relative abundance of typical intestinal bacteria is significantly enriched in samples obtained from patients diagnosed with aGVHD.

Supplementary Material 5: Supplementary Figure 5. aGVHD specific T cells exhibited characteristics of hyperactivated immune response.. Dot graph illustrating the results of KEGG analysis on the upregulated genes in αβ T cells derived from patients with aGVHD compared to those from individuals with non-aGVHD.. Volcano plots depicting differential gene expression profiles in various T cell subtypes between patients with non-aGVHD and those with aGVHD.. KEGG analysis was performed on the upregulated genes in αβ T cells from patients with non-aGVHD compared with those from individuals with aGVHD.

Supplementary Material 6: Supplementary Figure 6. Defensins are correlated to gut microbiota and bile acid metabolites in patients with allo-HSCT.. Dot plots illustrating the relative expression levels of *DEFB1*, *DEFA4*, and *DEFA3* in various subtypes of patients with aGVHD compared with individuals with non-aGVHD.. Heatmap showing the identified bile acid metabolites for each sample.. Heatmap showing the metabolites that exhibit the most significant differential expression.. Violin plots depicting the distribution of typical bile acid metabolites within each group.. The relationship between bile acid metabolites and gut microbiota is examined through Spearman's correlation coefficients. Positive correlations are denoted by red fields, while negative correlations are denoted by green fields. Statistical significance is indicated by *P < 0.05, with **denoting significance after Bonferroni correction.. The relative abundances of the typical bacteria were determined by applying of the t-test statistical method.

Supplementary Material 7: Supplementary Figure 7. GPBAR1 and NR1H2 are implicated in the regulation of immune responses.. Dot plots illustrating the varying expression levels of *GPBAR1*, *NR1H2*, *NR1I2*, and *NR1H4* across distinct cell subsets.. Dot plots illustrating the expression levels of *GPBAR1*, *NR1H2*, *NR1I2*, and *NR1H4* in myeloid cellsfrom various patients with aGVHD and control individuals with non-aGVHD.. Dot plots showing the expression levels of *GPBAR1*, *NR1H2*, *NR1I2*, *NR1H4*, as well as lineage-specific markersacross various cell subsets.. UMAP presenting the myeloid subsets, pseudotime analysis, and expression patterns of *NR1H2* and *GPBAR1*.. Volcano plots showing the upregulated and downregulated DEGs in *GPBAR1* and *NR1H2*-expressing CD14$^+$CD16$^-$ and CD14$^+$CD16$^+$ monocytes relative to their respective control groups.. Volcano plots and Dot plots showing the upregulated and downregulated DEGs in DC expressing *GPBAR1* and *NR1H2*, as compared to DC not expressing these genes.. UMAP presenting the granulocyte-like subsets.. Dot plots showing the expression levels of specific geneswithin various granulocyte-like subsets.. Volcano plots were utilized to display the upregulated and downregulated DEGs in granulocyte-like subsets expressing *GPBAR1* and *NR1H2*in comparison to their respective counterparts.

Supplementary Material 8: Supplementary Figure 8. Selected genes in bone marrow cells and splenic cells from a mouse model of aGVHD assessed using qPCR.

Supplementary Material 9: Supplementary Figure 9. Study design.

Supplementary Material 10.

Author contributions
Conceptualization: L.J.H., R.Q.G, and Y.J.; methodology: X.L.S., L.J.H., Y.X.G., R.Q.G., J.J.K., Y.W.Z., and J.L.; investigation and formal analysis: K.F., J.W.Z., Z.H.Z., F.Y.Y, Q.Z.C., M.M.Z., B.H.Y., X.Q.W., L.Y.F., Y.Y.C., Q.K.Y., S.Y.W., Q.X.X., N.N.S. Y.L.B., X.J.W., and D.F.Z.; funding Acquisition: R.Q.G., and L.J.H; supervision: Y.J., R.Q.G. and Y.X.G.; visualization and writing—original draft: R.Q.G. and L.J.H.; writing—review and editing: X.L.S., R.Q.G., L.J.H., and Y.J. All authors read and approved the final manuscript.

Availability of data and materials
All data needed to evaluate the conclusions in the paper are present in the paper and/or the Supplementary Materials. Sequence data are available from the National Genomics Data Center (NGDC), Genome Sequence Archive (GSA) database under the accession numbers HRA007481 (patients with aGVHD or non-aGVHD) and HRA005145 (healthy donors).

Declarations

Ethics approval and consent to participate
All procedures performed in studies involving human participants were approved by the Research and Clinical Trial Ethics Committee of the First Affiliated Hospital of ZZU (2023-KY-0778-002). The participants consented by providing a signature to collect and analyze biospecimens. Animal experiments were approved by the Ethical Committee of Zhengzhou University (ZZU-LAC20210604[06]).

Consent for publication
All authors approved the manuscript and gave their consent for submission and publication.

Competing interests
The authors declare that they have no competing interests.

Author details
[1]Translational Medical Center, The First Affiliated Hospital of Zhengzhou University, Zhengzhou, Henan, China. [2]Department of Hematology, The First Affiliated Hospital of Zhengzhou University, Zhengzhou, Henan, China. [3]Basic Medical Research Center, Academy of Medical Sciences, Zhengzhou University, Zhengzhou, Henan, China. [4]Department of Hematology, Henan Provincial People's Hospital, Zhengzhou University People's Hospital, Zhengzhou, Henan, China. [5]Department of Hematology, The Third People's Hospital of Zhengzhou, Zhengzhou 450000, Henan, China. [6]Department of Laboratory Medicine, The First Affiliated Hospital of Zhengzhou University, Zhengzhou, Henan, China. [7]Department of Laboratory Medicine, The First Affiliated Hospital of Henan University of Chinese Medicine, Zhengzhou, Henan, China. [8]Department of Blood Transfusion, The First Affiliated Hospital of Zhengzhou University, Zhengzhou, Henan, China. [9]Department of Emergency Medicine, The First Affiliated Hospital of Zhengzhou University, Zhengzhou, Henan, China. [10]Henan Key Laboratory of Critical Care Medicine, Department of Critical Care Medicine and Department of Emergency Medicine, The First Affiliated Hospital of Zhengzhou University, Zhengzhou, Henan, China.

References
1. Ali I, Wani WA, Saleem K, Hsieh M-F. Anticancer metallodrugs of glutamic acid sulphonamides: in silico, DNA binding, hemolysis and anticancer studies. RSC Adv. 2014;4(56):29629–41.

Han *et al. Journal of Translational Medicine*   (2024) 22:746

Page 22 of 24

2. Ali I, Wani WA, Haque A, Saleem K. Glutamic acid and its derivatives: candidates for rational design of anticancer drugs. Future Med Chem. 2013;5(8):961–78.

3. Ali I, Aboul-Enein YH, Ghanem A. Enantioselective toxicity and carcinogenesis. Curr Pharm Anal. 2005;1(1):109–25.

4. Koyama M, Mukhopadhyay P, Schuster IS, Henden AS, Hülsdünker J, Varelias A, Vetizou M, Kuns RD, Robb RJ, Zhang P, et al. MHC class II antigen presentation by the intestinal epithelium initiates graft-versus-host disease and is influenced by the microbiota. Immunity. 2019;51(5):885-898.e887.

5. Ali I, Wani WA, Khan A, Haque A, Ahmad A, Saleem K, Manzoor N. Synthesis and synergistic antifungal activities of a pyrazoline based ligand and its copper(II) and nickel(II) complexes with conventional antifungals. Microb Pathog. 2012;53(2):66–73.

6. Lin D, Hu B, Li P, Zhao Y, Xu Y, Wu D. Roles of the intestinal microbiota and microbial metabolites in acute GVHD. Exp Hematol Oncol. 2021;10(1):49.

7. Hill GR, Teshima T, Gerbitz A, Pan L, Cooke KR, Brinson YS, Crawford JM, Ferrara JL. Differential roles of IL-1 and TNF-alpha on graft-versus-host disease and graft versus leukemia. J Clin Invest. 1999;104(4):459–67.

8. Ferrara JLM, Levine JE. A new approach to therapy for acute GVHD. Cell Ther Transplant. 2008;1(1):25–7.

9. Zhao C, Zhang Y, Zheng H. The effects of interferons on allogeneic T cell response in GVHD: the multifaced biology and epigenetic regulations. Front Immunol. 2021;12: 717540.

10. Lindner S, Miltiadous O, Ramos RJF, Paredes J, Kousa AI, Dai A, Fei T, Lauder E, Frame J, Waters NR, et al. Altered microbial bile acid metabolism exacerbates T cell-driven inflammation during graft-versus-host disease. Nat Microbiol. 2024;9(3):614–30.

11. Koyama M, Hippe DS, Srinivasan S, Proll SC, Miltiadous O, Li N, Zhang P, Ensbey KS, Hoffman NG, Schmidt CR, et al. Intestinal microbiota controls graft-versus-host disease independent of donor-host genetic disparity. Immunity. 2023;56(8):1876-1893.e1878.

12. Gao F, Wu H, Wang L, Zhao Y, Huang H. Altered intestinal microbiome and epithelial damage aggravate intestinal graft-versus-host disease. Gut Microbes. 2023;15(1):2221821.

13. Chen X, Zhang Z, Sun N, Li J, Ma Z, Rao Z, Sun X, Zeng Q, Wu Y, Li J, et al. Vitamin D receptor enhances NLRC4 inflammasome activation by promoting NAIPs-NLRC4 association. EMBO Rep. 2022;23(9): e54611.

14. Qing F, Liu Z. Interferon regulatory factor 7 in inflammation, cancer and infection. Front Immunol. 2023;14:1190841.

15. Feng H, Zhang YB, Gui JF, Lemon SM, Yamane D. Interferon regulatory factor 1 (IRF1) and anti-pathogen innate immune responses. PLoS Pathog. 2021;17(1): e1009220.

16. Tian Y, Meng L, Wang Y, Li B, Yu H, Zhou Y, Bui T, Abraham C, Li A, Zhang Y, et al. Graft-versus-host disease depletes plasmacytoid dendritic cell progenitors to impair tolerance induction. J Clin Invest. 2021. https://doi.org/10.1172/JCI136774.

17. Li Q, Lan P. Activation of immune signals during organ transplantation. Signal Transduct Target Ther. 2023;8(1):110.

18. Gupta P, Barthwal MK. IL-1 β genesis: the art of regulating the regulator. Cell Mol Immunol. 2018;15(11):998–1000.

19. Shrestha B, Walton K, Reff J, Sagatys EM, Tu N, Boucher J, Li G, Ghafoor T, Felices M, Miller JS, et al. Human CD83-targeted chimeric antigen receptor T cells prevent and treat graft-versus-host disease. J Clin Investig. 2020;130(9):4652–62.

20. Holtan SG, Savid-Frontera C, Walton K, Eaton AA, Demorest C, Hoeschen A, Zhang L, Reid K, Kurian T, Sayegh Z, et al. Human effectors of acute and chronic GVHD overexpress CD83 and predict mortality. Clin Cancer Res. 2023;29(6):1114–24.

21. Tabellini L, Fan W, Zhao LP, Hansen JA. Identifying biomarkers for acute GVHD. Blood. 2006;108(11):38–38.

22. Son YM, Ahn SM, Jang MS, Moon YS, Kim SH, Cho KK, Han SH, Yun CH. Immunomodulatory effect of resistin in human dendritic cells stimulated with lipoteichoic acid from *Staphylococcus aureus*. Biochem Biophys Res Commun. 2008;376(3):599–604.

23. Son YM, Ahn SM, Kim GR, Moon YS, Kim SH, Park YM, Lee WK, Min TS, Han SH, Yun CH. Resistin enhances the expansion of regulatory T cells through modulation of dendritic cells. BMC Immunol. 2010;11:33.

24. Propheter DC, Chara AL, Harris TA, Ruhn KA, Hooper LV. Resistin-like molecule β is a bactericidal protein that promotes spatial segregation of the microbiota and the colonic epithelium. Proc Natl Acad Sci USA. 2017;114(42):11027–33.

25. Tarkowski A, Bjersing J, Shestakov A, Bokarewa MI. Resistin competes with lipopolysaccharide for binding to toll-like receptor 4. J Cell Mol Med. 2010;14(6b):1419–31.

26. Cui W, Guo M, Liu D, Xiao P, Yang C, Huang H, Liang C, Yang Y, Fu X, Zhang Y, et al. Gut microbial metabolite facilitates colorectal cancer development via ferroptosis inhibition. Nat Cell Biol. 2024;26(1):124–37.

27. Zhang H, Yang Z, Yuan W, Liu J, Luo X, Zhang Q, Li Y, Chen J, Zhou Y, Lv J, et al. Sustained AhR activity programs memory fate of early effector CD8+ T cells. Proc Natl Acad Sci. 2024;121(11): e2317658121.

28. Liu Y, Zhou N, Zhou L, Wang J, Zhou Y, Zhang T, Fang Y, Deng J, Gao Y, Liang X, et al. IL-2 regulates tumor-reactive CD8+ T cell exhaustion by activating the aryl hydrocarbon receptor. Nat Immunol. 2021;22(3):358–69.

29. Campesato LF, Budhu S, Tchaicha J, Weng C-H, Gigoux M, Cohen IJ, Redmond D, Mangarin L, Pourpe S, Liu C, et al. Blockade of the AHR restricts a Treg-macrophage suppressive axis induced by ʟ-kynurenine. Nat Commun. 2020;11(1):4011.

30. Bessede A, Gargaro M, Pallotta MT, Matino D, Servillo G, Brunacci C, Bicciato S, Mazza EM, Macchiarulo A, Vacca C, et al. Aryl hydrocarbon receptor control of a disease tolerance defence pathway. Nature. 2014;511(7508):184–90.

31. Kim Y-G, Sakamoto K, Seo S-U, Pickard JM, Gillilland MG, Pudlo NA, Hoostal M, Li X, Wang TD, Feehley T, et al. Neonatal acquisition of *Clostridia* species protects against colonization by bacterial pathogens. Science. 2017;356(6335):315–9.

32. Zhu X, Shen J, Feng S, Huang C, Wang H, Huo F, Liu H. *Akkermansia muciniphila*, which is enriched in the gut microbiota by metformin, improves cognitive function in aged mice by reducing the proinflammatory cytokine interleukin-6. Microbiome. 2023;11(1):120.

33. Bae M, Cassilly CD, Liu X, Park S-M, Tusi BK, Chen X, Kwon J, Filipčík P, Bolze AS, Liu Z, et al. *Akkermansia muciniphila* phospholipid induces homeostatic immune responses. Nature. 2022;608(7921):168–73.

34. Li F, Hao X, Chen Y, Bai L, Gao X, Lian Z, Wei H, Sun R, Tian Z. The microbiota maintain homeostasis of liver-resident γδT-17 cells in a lipid antigen/CD1d-dependent manner. Nat Commun. 2017;8(1):13839.

35. Fang Y, Zhu Y, Kramer A, Chen Y, Li YR, Yang L. Graft-versus-host disease modulation by innate T cells. Int J Mol Sci. 2023;24(4):4084.

36. Mogilenko DA, Shpynov O, Andhey PS, Arthur L, Swain A, Esaulova E, Brioschi S, Shchukina I, Kerndl M, Bambouskova M, et al. Comprehensive profiling of an aging immune system reveals clonal GZMK(+) CD8(+) T cells as conserved hallmark of inflammaging. Immunity. 2021;54(1):99-115.e112.

37. Guo R, Kong J, Tang P, Wang S, Sang L, Liu L, Guo R, Yan K, Qi M, Bian Z, et al. Unbiased single-cell sequencing of hematopoietic and immune cells from aplastic anemia reveals the contributors of hematopoiesis failure and dysfunctional immune regulation. Adv Sci. 2024;11(10):2304539.

38. Li J, Zaslavsky M, Su Y, Guo J, Sikora MJ, van Unen V, Christophersen A, Chiou SH, Chen L, Li J, et al. KIR(+)CD8(+) T cells suppress pathogenic T cells and are active in autoimmune diseases and COVID-19. Science. 2022;376(6590): eabi9591.

39. Rückert T, Andrieux G, Boerries M, Hanke-Müller K, Woessner NM, Doetsch S, Schell C, Aumann K, Kolter J, Schmitt-Graeff A, et al. Human β-defensin 2 ameliorates acute GVHD by limiting ileal neutrophil infiltration and restraining T cell receptor signaling. Sci Transl Med. 2022;14(676): eabp9675.

40. Larabi AB, Masson HLP, Bäumler AJ. Bile acids as modulators of gut microbiota composition and function. Gut Microbes. 2023;15(1):2172671.

41. Tremblay S, Romain G, Roux M, Chen X-L, Brown K, Gibson DL, Ramanathan S, Menendez A. Bile acid administration elicits an intestinal antimicrobial program and reduces the bacterial burden in two mouse models of enteric infection. Infect Immunity. 2017;85(6):10–128. https://doi.org/10.1128/iai.00942-00916.

42. Wang S, Kuang J, Zhang H, Chen W, Zheng X, Wang J, Huang F, Ge K, Li M, Zhao M, et al. Bile acid-microbiome interaction promotes gastric carcinogenesis. Adv Sci. 2022;9(16):2200263.

43. Xie G, Jiang R, Wang X, Liu P, Zhao A, Wu Y, Huang F, Liu Z, Rajani C, Zheng X, et al. Conjugated secondary 12α-hydroxylated bile acids promote liver fibrogenesis. EBioMedicine. 2021;66: 103290.

Han *et al. Journal of Translational Medicine*   (2024) 22:746

Page 23 of 24

44. Zhong J, He X, Gao X, Liu Q, Zhao Y, Hong Y, Zhu W, Yan J, Li Y, Li Y, et al. Hyodeoxycholic acid ameliorates nonalcoholic fatty liver disease by inhibiting RAN-mediated PPARα nucleus-cytoplasm shuttling. Nat Commun. 2023;14(1):5451.

45. Xiao R, Lei K, Kuok H, Deng W, Zhuang Y, Tang Y, Guo Z, Qin H, Bai LP, Li T. Synthesis and identification of lithocholic acid 3-sulfate as RORγt ligand to inhibit Th17 cell differentiation. J Leukoc Biol. 2022;112(4):835–43.

46. Li N, Ma P, Li Y, Shang X, Nan X, Shi L, Han X, Liu J, Hong Y, Li Q, et al. Gut microbiota-derived 12-ketolithocholic acid suppresses the IL-17A secretion from colonic group 3 innate lymphoid cells to prevent the acute exacerbation of ulcerative colitis. Gut Microbes. 2023;15(2):2290315.

47. Hoque R, Sohail M, Malik A, Sarwar S, Luo Y, Shah A, Barrat F, Flavell R, Gorelick F, Husain S, et al. TLR9 and the NLRP3 inflammasome link acinar cell death with inflammation in acute pancreatitis. Gastroenterology. 2011;141(1):358–69.

48. Ziegler F, Steuer A, Di Pizio A, Behrens M. Physiological activation of human and mouse bitter taste receptors by bile acids. Commun Biol. 2023;6(1):612.

49. Calzadilla N, Comiskey SM, Dudeja PK, Saksena S, Gill RK, Alrefai WA. Bile acids as inflammatory mediators and modulators of intestinal permeability. Front Immunol. 2022;13:1021924.

50. Campbell C, McKenney PT, Konstantinovsky D, Isaeva OI, Schizas M, Verter J, Mai C, Jin W-B, Guo C-J, Violante S, et al. Bacterial metabolism of bile acids promotes generation of peripheral regulatory T cells. Nature. 2020;581(7809):475–9.

51. Shen X, Dong P, Kong G, Sun N, Wang F, Sang L, Xu Y, Zhang M, Chen X, Guo R, et al. Targeted single-cell RNA sequencing analysis reveals metabolic reprogramming and the ferroptosis-resistant state in hematologic malignancies. Cell Biochem Funct. 2023;41(8):1343–56.

52. Guo R, Li W, Li Y, Li Y, Jiang Z, Song Y. Generation and clinical potential of functional T lymphocytes from gene-edited pluripotent stem cells. Exp Hematol Oncol. 2022;11(1):27.

53. Zhang D, Li Y, Du C, Sang L, Liu L, Li Y, Wang F, Fan W, Tang P, Zhang S, et al. Evidence of pyroptosis and ferroptosis extensively involved in autoimmune diseases at the single-cell transcriptome level. J Transl Med. 2022;20(1):363.

54. Li Y, Cao H, Jiang Z, Yan K, Shi J, Wang S, Wang F, Wang W, Li X, Sun N, et al. CCL17 acts as an antitumor chemokine in micromilieu-driven immune skewing. Int Immunopharmacol. 2023;118: 110078.

55. Jarosch S, Köhlen J, Ghimire S, Orberg ET, Hammel M, Gaag D, Evert M, Janssen KP, Hiergeist A, Gessner A, et al. Multimodal immune cell phenotyping in GI biopsies reveals microbiome-related T cell modulations in human GvHD. Cell Rep Med. 2023;4(7): 101125.

56. Engel JA, Lee HJ, Williams CG, Kuns R, Olver S, Lansink LI, Soon MS, Andersen SB, Powell JE, Svensson V, et al. Single-cell transcriptomics of alloreactive CD4+ T cells over time reveals divergent fates during gut graft-versus-host disease. JCI Insight. 2020;5(13): e137990.

57. de Almeida GP, Lichtner P, Eckstein G, Brinkschmidt T, Chu C-F, Sun S, Reinhard J, Mädler SC, Kloeppel M, Verbeek M, et al. Human skin-resident host T cells can persist long term after allogeneic stem cell transplantation and maintain recirculation potential. Sci Immunol. 2022;7(67): eabe2634.

58. Strobl J, Gail LM, Krecu L, Madad S, Kleissl L, Unterluggauer L, Redl A, Brazdilova K, Saluzzo S, Wohlfarth P, et al. Diverse macrophage populations contribute to distinct manifestations of human cutaneous graft-versus-host disease. Br J Dermatol. 2023;190(3):402–14.

59. Zhao W, Wang Y, Zhang X, Hao J, Zhang K, Huang X, Chang Y, Wu H, Jin R, Ge Q. Impaired thymic iNKT cell differentiation at early precursor stage in murine haploidentical bone marrow transplantation with GvHD. Front Immunol. 2023;14:1203614.

60. Tkachev V, Kaminski J, Potter EL, Furlan SN, Yu A, Hunt DJ, McGuckin C, Zheng H, Colonna L, Gerdemann U, et al. Spatiotemporal single-cell profiling reveals that invasive and tissue-resident memory donor CD8+ T cells drive gastrointestinal acute graft-versus-host disease. Sci Transl Med. 2021;13(576): eabc0227.

61. Obermayer B, Keilholz L, Conrad T, Frentsch M, Blau I-W, Vuong L, Lesch S, Movasshagi K, Tietze-Stolley C, Loyal L, et al. Single-cell clonal tracking of persistent T-cells in allogeneic hematopoietic stem cell transplantation. Front Immunol. 2023;14:1114368.

62. Hess NJ, Turicek DP, Riendeau J, McIlwain SJ, Contreras Guzman E, Nadiminti K, Hudson A, Callander NS, Skala MC, Gumperz JE, et al. Inflammatory CD4/CD8 double-positive human T cells arise from reactive CD8 T cells and are sufficient to mediate GVHD pathology. Sci Adv. 2023;9(12): eadf0567.

63. Zheng J, Liu Y, Liu Y, Liu M, Xiang Z, Lam K-T, Lewis DB, Lau Y-L, Tu W. Human CD8+ regulatory T cells inhibit GVHD and preserve general immunity in humanized mice. Sci Transl Med. 2013;5(168):168ra169.

64. Miyagawa F, Okiyama N, Villarroel V, Katz SI. Identification of CD3+CD4− CD8− T cells as potential regulatory cells in an experimental murine model of graft-versus-host skin disease (GVHD). J Invest Dermatol. 2013;133(11):2538–45.

65. Khandelwal P, Chaturvedi V, Owsley E, Lane A, Heyenbruch D, Lutzko CM, Leemhuis T, Grimley MS, Nelson AS, Davies SM, et al. CD38(bright)CD8(+) T cells associated with the development of acute GVHD are activated, proliferating, and cytotoxic trafficking cells. Biol Blood Marrow Transplant. 2020;26(1):1–6.

66. Gartlan KH, Markey KA, Varelias A, Bunting MD, Koyama M, Kuns RD, Raffelt NC, Olver SD, Lineburg KE, Cheong M, et al. Tc17 cells are a proinflammatory, plastic lineage of pathogenic CD8+ T cells that induce GVHD without antileukemic effects. Blood. 2015;126(13):1609–20.

67. Lynn RC, Weber EW, Sotillo E, Gennert D, Xu P, Good Z, Anbunathan H, Lattin J, Jones R, Tieu V, et al. c-Jun overexpression in CAR T cells induces exhaustion resistance. Nature. 2019;576(7786):293–300.

68. Yukawa M, Jagannathan S, Vallabh S, Kartashov AV, Chen X, Weirauch MT, Barski A. AP-1 activity induced by co-stimulation is required for chromatin opening during T cell activation. J Exp Med. 2020;217(1): e20182009.

69. Yang H, Xia L, Chen J, Zhang S, Martin V, Li Q, Lin S, Chen J, Calmette J, Lu M, et al. Stress–glucocorticoid–TSC22D3 axis compromises therapy-induced antitumor immunity. Nat Med. 2019;25(9):1428–41.

70. Asselin-Labat M-L, David M, Biola-Vidamment A, Lecoeuche D, Zennaro M-C, Bertoglio J, Pallardy M. GILZ, a new target for the transcription factor FoxO3, protects T lymphocytes from interleukin-2 withdrawal-induced apoptosis. Blood. 2004;104(1):215–23.

71. Zhang Y, Reynolds JM, Chang SH, Martin-Orozco N, Chung Y, Nurieva RI, Dong C. MKP-1 is necessary for T cell activation and function. J Biol Chem. 2009;284(45):30815–24.

72. Lu D, Liu L, Ji X, Gao Y, Chen X, Liu Y, Liu Y, Zhao X, Li Y, Li Y, et al. The phosphatase DUSP2 controls the activity of the transcription activator STAT3 and regulates TH17 differentiation. Nat Immunol. 2015;16(12):1263–73.

73. Kye Y-C, Lee G-W, Lee S-W, Ju Y-J, Kim H-O, Yun C-H, Cho J-H. STAT1 maintains naïve CD8+ T cell quiescence by suppressing the type I IFN-STAT4-mTORC1 signaling axis. Sci Adv. 2021;7(36): eabg8764.

74. DeDiego ML, Martinez-Sobrido L, Topham DJ. Novel functions of IFI44L as a feedback regulator of host antiviral responses. J Virol. 2019;93(21):10–128.

75. Palmer DC, Webber BR, Patel Y, Johnson MJ, Kariya CM, Lahr WS, Parkhurst MR, Gartner JJ, Prickett TD, Lowery FJ, et al. Internal checkpoint regulates T cell neoantigen reactivity and susceptibility to PD1 blockade. Med. 2022;3(10):682-704.e688.

76. Wang F, Zhao S, Gu Z, Zhao X, Yang N, Guan L, Liu T, Wang L, Fang S, Zhu C, et al. S1PR5 regulates NK cell responses in preventing graft-versus-host disease while preserving graft-versus-tumour activity in a murine allogeneic haematopoietic stem cell transplantation model. Hematol Oncol. 2020;38(1):89–102.

77. Hsiao C-C, Kragten NAM, Piao X, Hamann J, van Gisbergen KPJM. The inhibitory receptor GPR56 (Adgrg1) is specifically expressed by tissue-resident memory T cells in mice but dispensable for their differentiation and function in vivo. Cells. 2021;10(10):2675.

78. Huo Y, Wu L, Pang A, Li Q, Hong F, Zhu C, Yang Z, Dai W, Zheng Y, Meng Q, et al. Single-cell dissection of human hematopoietic reconstitution after allogeneic hematopoietic stem cell transplantation. Sci Immunol. 2023;8(81): eabn6429.

79. Yang Y, Cadwell K. Beyond antiviral: interferon induced by bacteria maintains tolerance in the gut. J Exp Med. 2023;221(1): e20232011.

80. Vasquez Ayala A, Hsu CY, Oles RE, Matsuo K, Loomis LR, Buzun E, Carrillo Terrazas M, Gerner RR, Lu HH, Kim S, et al. Commensal bacteria promote type I interferon signaling to maintain immune tolerance in mice. J Exp Med. 2024;221(1): e20230063.

81. Andreakos E. Type I and type III interferons: from basic biology and genetics to clinical development for COVID-19 and beyond. Semin Immunol. 2024;72: 101863.

Han *et al. Journal of Translational Medicine*   (2024) 22:746

Page 24 of 24

82. Williams M, Mejaki B, Graff J, Sana S, Medlin S, Gul Z. Use of type 1 interferon-alpha 2a for relapse prevention in allogeneic stem cell transplant. Transpl Cell Ther. 2024;30(2):S401–2.

83. Guarda G, Braun M, Staehli F, Tardivel A, Mattmann C, Förster I, Farlik M, Decker T, Du Pasquier RA, Romero P, et al. Type I interferon inhibits interleukin-1 production and inflammasome activation. Immunity. 2011;34(2):213–23.

84. Hamarsheh S, Zeiser R. Chapter 26—The inflammasome in graft-versus-host disease. In: Pelegrin P, editor. Inflammasome biology. New York: Academic Press; 2023. p. 421–6.

85. Seo S-U, Kamada N, Muñoz-Planillo R, Kim Y-G, Kim D, Koizumi Y, Hasegawa M, Himpsl Stephanie D, Browne Hilary P, Lawley Trevor D, et al. Distinct commensals induce interleukin-1β via NLRP3 inflammasome in inflammatory monocytes to promote intestinal inflammation in response to injury. Immunity. 2015;42(4):744–55.

86. Li Y, Yang Q, Cai D, Guo H, Fang J, Cui H, Gou L, Deng J, Wang Z, Zuo Z. Resistin, a novel host defense peptide of innate immunity. Front Immunol. 2021;12: 699807.

87. Eriguchi Y, Takashima S, Oka H, Shimoji S, Nakamura K, Uryu H, Shimoda S, Iwasaki H, Shimono N, Ayabe T, et al. Graft-versus-host disease disrupts intestinal microbial ecology by inhibiting Paneth cell production of α-defensins. Blood. 2012;120(1):223–31.

88. Shono Y, Docampo MD, Peled JU, Perobelli SM, Velardi E, Tsai JJ, Slingerland AE, Smith OM, Young LF, Gupta J, et al. Increased GVHD-related mortality with broad-spectrum antibiotic use after allogeneic hematopoietic stem cell transplantation in human patients and mice. Sci Transl Med. 2016;8(339):339ra371.

89. Ingham AC, Kielsen K, Cilieborg MS, Lund O, Holmes S, Aarestrup FM, Müller KG, Pamp SJ. Specific gut microbiome members are associated with distinct immune markers in pediatric allogeneic hematopoietic stem cell transplantation. Microbiome. 2019;7(1):131.

90. Xia C, Su J, Liu C, Mai Z, Yin S, Yang C, Fu L. Human microbiomes in cancer development and therapy. MedComm. 2023;4(2): e221.

91. Li Y, Xu H, Zhou L, Zhang Y, Yu W, Li S, Gao J. Bifidobacterium breve protects the intestinal epithelium and mitigates inflammation in colitis via regulating the gut microbiota-cholic acid pathway. J Agric Food Chem. 2024;72(7):3572–83.

92. Jiao N, Loomba R, Yang Z-H, Wu D, Fang S, Bettencourt R, Lan P, Zhu R, Zhu L. Alterations in bile acid metabolizing gut microbiota and specific bile acid genes as a precision medicine to subclassify NAFLD. Physiol Genom. 2021;53(8):336–48.

93. Zhao M, Zhang X, Wang F, Hu X, Xue Z, Yue J, Chen M. A multiomics analysis of the close connection between intratumoral microbiota and immune cell infiltration in colorectal cancer. Int J Radiat Oncol Biol Phys. 2023;117(2): e358.

94. Xiao F, Gao X, Hu H, Le J, Chen Y, Shu X, Liang Z, Xu Y, Wang Y, Zhang T. Exclusive enteral nutrition exerts anti-inflammatory effects through modulating microbiota, bile acid metabolism, and immune activities. Nutrients. 2022;14(21):4463.

95. Han L, Zhao K, Li Y, Han H, Zhou L, Ma P, Fan Z, Sun H, Jin H, Jiang Z, et al. A gut microbiota score predicting acute graft-versus-host disease following myeloablative allogeneic hematopoietic stem cell transplantation. Am J Transplant. 2020;20(4):1014–27.

96. Lawlor N, Nehar-Belaid D, Grassmann JDS, Stoeckius M, Smibert P, Stitzel ML, Pascual V, Banchereau J, Williams A, Ucar D. Single cell analysis of blood mononuclear cells stimulated through either LPS or anti-CD3 and anti-CD28. Front Immunol. 2021;12: 636720.

97. Bu X, Wang J, Yin Z, Pan W, Liu L, Jin H, Liu Q, Zheng L, Sun H, Gao Y, et al. Human amniotic mesenchymal stem cells alleviate aGVHD after allo-HSCT by regulating interactions between gut microbiota and intestinal immunity. Stem Cell Rev Rep. 2023;19(5):1370–83.

98. Zhang X, He J, Zhao K, Liu S, Xuan L, Chen S, Xue R, Lin R, Xu J, Zhang Y, et al. Mesenchymal stromal cells ameliorate chronic GVHD by boosting thymic regeneration in a CCR9-dependent manner in mice. Blood Adv. 2023;7(18):5359–73.

Publisher's Note